Marine Structures 90 (2023) 103429

Contents lists available at ScienceDirect

Marine Structures

journal homepage: www.elsevier.com/locate/marstruc

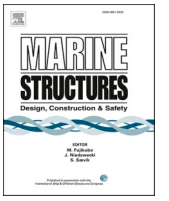

Stress concentration factors in FRP-reinforced tubular DKT joints under axial loads

E. Zavvar [a], J. Henneberg [b], C. Guedes Soares [a,1,*]

[a] Centre for Marine Technology and Ocean Engineering (CENTEC), Instituto Superior Técnico, Universidade de Lisboa, Portugal
[b] Faculty of Civil Engineering and Geodetic Science, Leibniz University Hannover, Hannover, 30167, Germany

ARTICLE INFO

Keywords:
Uniplanar DKT-Joints
Stress concentration factor
Axial loads
Fibre-reinforced polymer

ABSTRACT

The stress concentration factors (SCFs) in uniplanar fibre-reinforced polymer (FRP) DKT joints are calculated under five axial loading conditions to determine the maximum SCFs. To this end, 108 finite element models of reinforced DKT joints with different FRPs and geometrical parameters are analysed. Available experimental data and formulas are used to validate the finite element models. The validated finite element models are utilized to investigate the effects of the FRP parameters along with different geometrical parameters on the stress concentration factors in uniplanar DKT joints. The simulations show a reduction of the maximum SCF by around 40% compared to unreinforced DKT joints. The reduction effect increases significantly with increasing the FRP thickness and the number of layers. Despite the notable efficacy of the FRP sheets on the drop of the SCFs in the X-connections, there is not any study or equation on the X-joints with FRP. Therefore, a precise equation is proposed for quantifying the SCFs in X-connections with FRP and is checked against the UK DoE acceptance standard.

1. Introduction

Tubular steel structures are commonly used in many structures, namely offshore jackets, and bridges (Fig. 1). During their service life, they will be exposed to cyclic loadings which can create severe fatigue damage. Offshore jacket structures' service life depends in many cases on the structural integrity of the tubular joints. Hence, designing joints for service life and fatigue is the basis to ensure structural integrity.

One typical method to predict the fatigue resistance of tubular steel joints is the structural stress concept. Here, the S–N curves are based on hot spot stresses (HSSs) and SCFs [1]. The S–N curves are extensively utilized to predict fatigue life. As representative stresses nearby the notch HSSs are used [2]. The HSS range is responsible for the commencement of fatigue cracks, which will bring about the failure of joints. SCFs are defined as the ratio of hot spot stress to nominal stress [3].

Typical investigation procedures to determine the fatigue resistance of tubular joints are experimental and numerical analyses. Gao [4] studied numerically and experimentally the prediction of SCFs in T-joints (Fig. 1a) subjected to in-plane bending (IPB) loads. Cheng et al. [5] conducted a study on bird-beak SHS T-joints (Fig. 1a) under basic loads (Axial (AX), in-plane bending (IPB), and out-of-plane bending (OPB)) to determine SCFs and effects of dimensionless parameters. It was found that the dimensionless parameter β (the ratio of the brace diameter to the chord diameter) always increases the SCF of chord crown points. At saddle points, SCFs increase when γ

* Corresponding author.
E-mail address: c.guedes.soares@centec.tecnico.ulisboa.pt (C. Guedes Soares).
[1] ISSC2022 Standing Committee; ISSC-ITTC Joint Committee on Uncertainty Modelling.

https://doi.org/10.1016/j.marstruc.2023.103429
Received 27 December 2022; Received in revised form 6 February 2023; Accepted 21 February 2023
Available online 27 April 2023

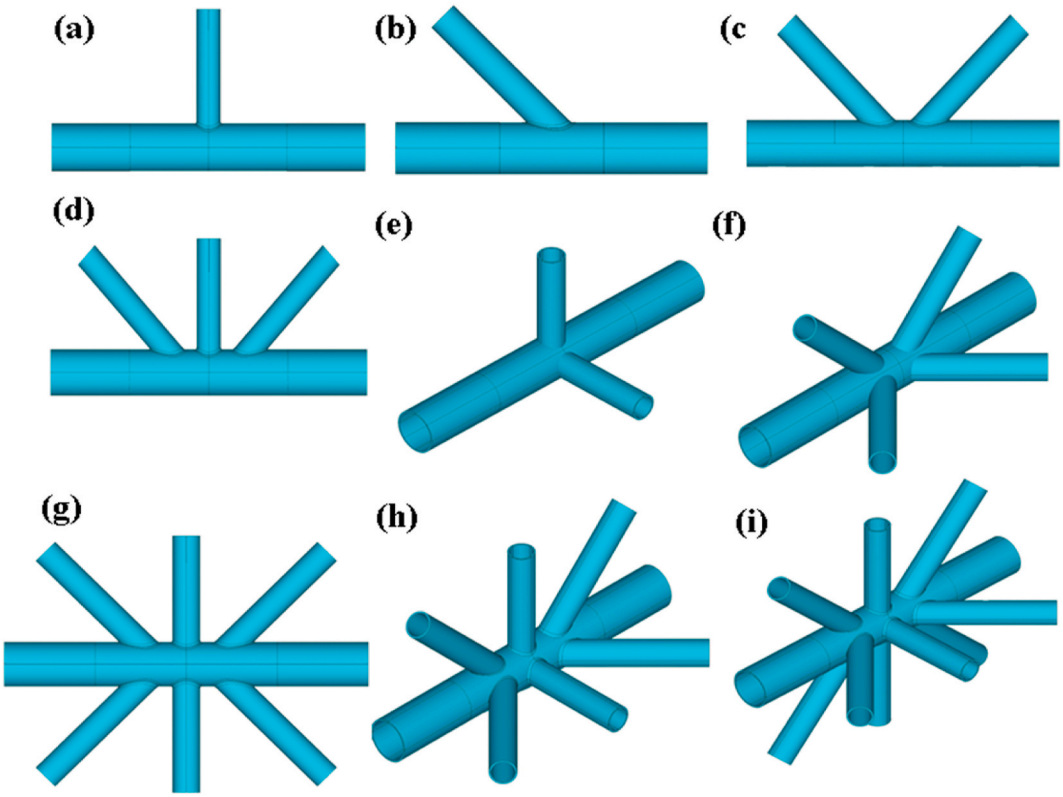

Fig. 1. Tubular joint classification: a) T; b) Y; c) K; d) KT; e) DT; f) DK; g) DKT; h) DKT; i) Three-planar KT.

(the ratio of the chord diameter to the chord thickness) increases. The increase of τ (the ratio of the thickness of the brace to the thickness of the chord) leads to an increase of SCF in all positions.

In another study by Shao [6], K-joints (Fig. 1c) subjected to balanced axial loads (AX) were investigated. After analyzing 1008 FE models, a set of equations was established to calculate SCFs based on dimensionless parameters. Zhang et al. [7] analysed overlapping KK-joints to obtain universal SCFs (Fig. 1f) under basic loading conditions by using shell elements in ANSYS. These universal SCFs for equivalent joint beam models can be obtained just based on basic loading conditions. This leads to savings in computation time, as traditional FE techniques are not necessary to predict SCF values in these kinds of tubular joints.

Liu et al. [8] studied KK-joints (Fig. 1f) to optimize the FE simulation method by using a stress influence matrix (SIM) method and a modified version of SIM (gSIM). They used these methods to simplify and save computation effort. They found that the gSIM method can reduce the computation time by 4000 times more than the FE simulation method. Jiang et al. [9] performed a research study to predict the effects of nondimensional parameters on DT joints (Fig. 1e) subjected to axial loads. They proposed equations to calculate SCFs for such joints and concluded that γ has a considerable effect on the SCFs compared to other parameters. Lotfollahi-Yaghin and Ahmadi [10] investigated tubular DKT joints (Fig. 1h) subjected to axial loading to evaluate the effects of dimensionless parameters on the SCFs. As a result, they developed equations to predict SCF values.

Ahmadi and Zavvar [11] and Zavvar et al. [12] conducted a research study on three-planar KT joints (Fig. 1i) under in-plane bending (IPB) and out-of-plane bending (OPB). They proposed equations to calculate SCFs in multi-planar KT joints. In another research study about KT joints (Fig. 1d), Ahmadi and Zavvar [13,14] investigated the degree of bending (DoB). A set of formulae has been proposed to determine DoB in KT joints subjected to AX, IPB, and OPB. To further understand SCFs in steel tubular KT joints, Ahmadi et al. [15] carried out a probabilistic study. They used Kolmogorov-Smirnov and Chi-squared tests to evaluate the quality of the fit of the SCF formulae under in-plane bending moments in KT joints. Ahmadi and Zavvar [16] performed research on ring-stiffened KT joints subjected to the out-of-plane bending (OPB) load. ANSYS software and SPSS were used to create 108 FE models with solid elements and to propose formulae to predict SCFs.

To reinforce and rehabilitate tubular structures, several methods are used, for example, internal rings [16], FRP [17], doubler plates [18], collar plates [19,20], brackets [21], concrete [22], grout [23], among others. Since many decades ago, composite materials have been used to build ships [24,25]]. As the advantages of composite materials, such as lightweight, corrosion resistance and superior strength became apparent, they have been used to strengthen steel structures at specific locations [26]. This has also occurred in offshore structures by reinforcing tubular joints with composites (Fig. 2).

Some investigations on the FRP strengthening approach were done by Zhao and Zhang [27], Yu et al. [28], and Lin et al. [29]. Xu et al. [30] studied CFRP-strengthened DT joints to propose formulae to evaluate SCFs by analysis of 704 FE models in ABAQUS. It was

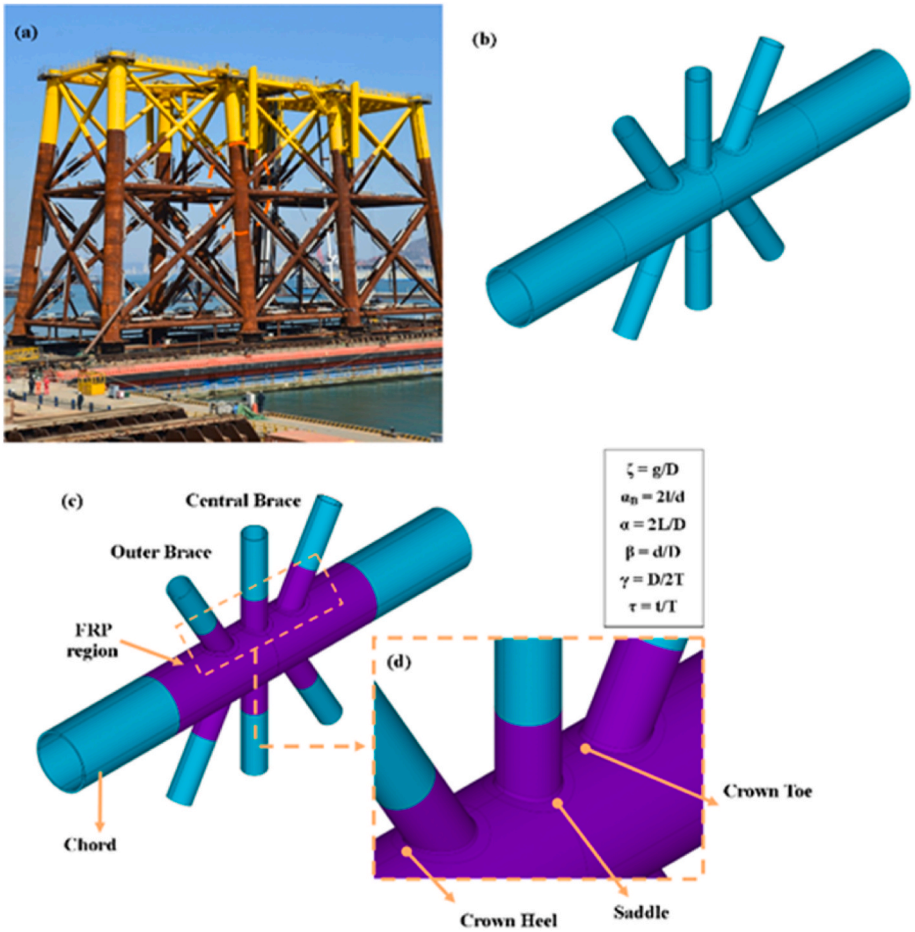

Fig. 2. A uniplanar DKT-joint, which is used in fixed offshore platforms; a) Uniplanar KT-joints in a platform; b) Unreinforced uniplanar KT-joints; c) Uniplanar KT-joints reinforced with FRP; d) saddle, crown toe, and crown heel positions.

concluded that the maximum SCF in CFRP-strengthened DT joints decreases compared to simple steel DT-joints by about 14%, and the fatigue life increases by about 47%. Hosseini et al. [31] performed a study on SCFs in reinforced KT joints (Fig. 1d). They conducted a numerical analysis by using FE models in ABAQUS under axial loading conditions to predict the effects of FRP and geometry parameters. Nassiraei and Rezadoost [32–34] conducted a comprehensive study on FRP-strengthened T/Y joints subjected to main loading conditions including compressive, in-plane bending, and out-of-plane bending loads. A total of 531 FE models with solid 186 and shell 286 in ANSYS software program were created and analysed to predict the effect of the FRP layer numbers, FRP layer materials, the joint geometry, and the brace angle (θ). They concluded that the SCF of an FRP-reinforced T/Y joint under compressive can be reduced to 34% of the SCF of the corresponding unreinforced joint FRP-strengthened T/Y joints, but in joints under in-plane bending loads reduction is about 40%, and in joints under out-of-plane bending loads reduction is about 29%. Zhao et al. [35] investigated rectangular hollow section (RHS) joints stiffened with FRP. A main finding was that CFRP significantly increases the

Table 1
Values of dimensionless parameters to describe the geometrical configuration of tubular joint.

Parameter	Definition	Value(s)
β	d/D	0.4, 0.5, 0.6, 0.7
γ	$D/2T$	12, 18, 24
τ	t/T	0.4, 0.7, 1.0
θ	–	30°, 45°, 60°
ζ	g/D	0.3
N	Number of FRP sheets	4, 8, 12, 16
ξ	E_{FRP}/E_{Steel}	0.14–0.87
η	T_{FRP}/T_{chord}	
α	$2\,L/D$	16
α_B	2 L/d	8

crippling web capacity. Zavvar et al. [36] carried out a study on KT-joint strengthened with FRP under bending moments. 2920 finite element models with solid elements were analysed in ABAQUS to propose formulae to determine their SCFs. Lesani et al. [37] conducted a numerical study on FRP- stiffened T-joints to predict the ultimate limit state capacity. Glass/vinyl ester was used to reinforce the joint. In other investigation, Nassiraei and Rezadoost [38,39] studied X-connections retrofitted with FRP under compressive and in-plane bending.

In this research, the effects of FRP on SCFs in uniplanar KT-joints reinforced with different fibre-reinforced polymers Glass/vinyl ester, Glass/epoxy (Scotchply 1002), S-glass/epoxy, Aramid/epoxy (Kevlar 9/Epoxy), Carbon/Epoxy (AS/3501), and Carbon/epoxy (T300/5208) under five axial loading conditions is numerically investigated. The main reason for conducting this research is the lack of investigations on SCFs of FRP-stiffened uniplanar KT joints. The commercial FE software ANSYS was used to create 5184 finite element models with different geometries defined by dimensionless parameters (Table 1), FRP materials, and several FRP layers/orientations. It is worth mentioning that these ranges of dimensionless parameters cover a large number of tubular connections utilized in offshore structures. Results of experimental tests conducted by Lloyd's Register of Shipping OTH 354 [40], Chiew et al. [41], Lloyd's Register of Shipping OTH 353 [42], Hosseini et al. [43], Tong et al. [44] and formulae proposed by the LR equations [40], and API code [45] were utilized for validation.

2. Finite element modelling

2.1. Loading and boundary conditions

Under the considered axial loads, symmetry boundary conditions are used to reduce the modelling effort and analyse only half the model (Fig. 3). This helps to reduce the stiffness matrix and the analysis time. The chord end fixity conditions of tubular joints in offshore structures range from almost fixed to almost pinned, generally being closer to almost fixed [46]. Based on the research studies carried out by Smedley and Fisher [47], both chord ends are fixed. Smedley and Fisher [49] showed that changing the end restraints of the joints affects the SCF values at the crown position up to +15% for joints with $\alpha = 6$ and 8% for $\alpha = 8$. Since the chord end fixity effect is only significant for joints with $\alpha < 8$ and high β and γ values, which do not commonly occur in practice, in this study, the α is assumed 16. A comparison of the effect of chord end fixity on SCF values in KT joints was conducted by Refs. [12,36], and results showed that fixed chord ends and pinned chord ends have less than 1% difference when $\alpha = 16$. Therefore, in this research, both chord ends were assumed to be fixed for all joints. Uniplanar KT-joints are analysed under 16 loading conditions (Table A-1 in the appendix) where 4 loading conditions (Table 2) create maximum SCFs. Hence, the number of loading conditions is reduced to the decisive 4 loading patterns according to Table 2. In addition, thanks to the symmetric or antisymmetric joints and loading conditions, SCFs are extracted for some points presented in Table A-2 at the appendix, and the location of extraction SCF points in the uniplanar DKT-joints is shown in Fig. 5. The numbering according to the loading patterns is shown in Fig. 4. The value of 1 and -1 represent compression and tension loading, respectively. The Young's modulus is 207 GPa, and the Poisson's ratio is 0.3.

2.2. Weld profile and mesh generation

A decisive parameter for the fatigue design is the dihedral angle Ψ (Fig. 6), which can be defined by equation (1) according to Refs. [16,48]:

$$\psi = \begin{cases} \pi/2 & Crown \\ \pi - \cos^{-1}\beta & Saddle \\ \pi - \theta & Crown\ toe \\ \theta & Crown\ heel \end{cases} \tag{1}$$

$$H_w(mm) = 0.85t(mm) + 4.24 \tag{2}$$

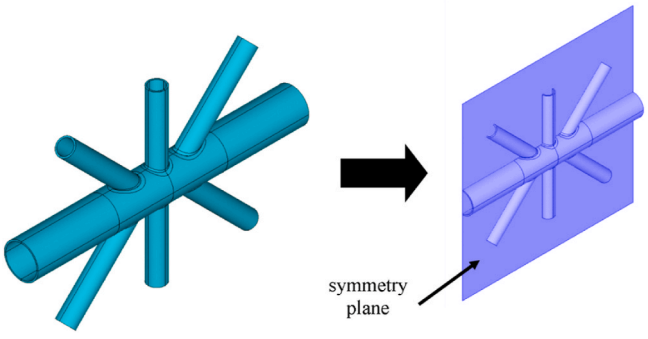

Fig. 3. Symmetry plane in created models.

Table 2
Applied loading patterns which create maximum SCFs.

No Loading	Brace					
	A	B	C	D	E	F
1	1	1	1	1	1	1
2	−1	1	−1	1	1	1
3	−1	−1	1	1	1	1
4	1	1	1	−1	−1	−1

1 = Compression, −1 = Tension.

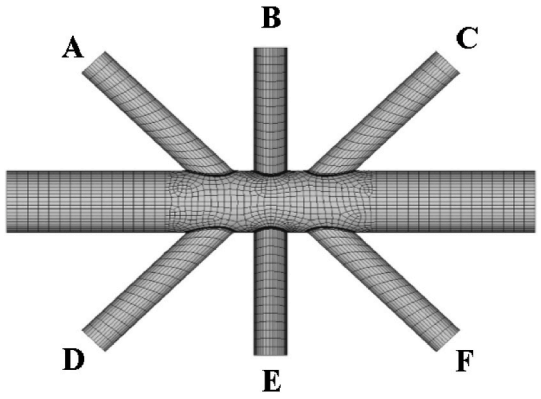

Fig. 4. Designation of braces for different loading patterns.

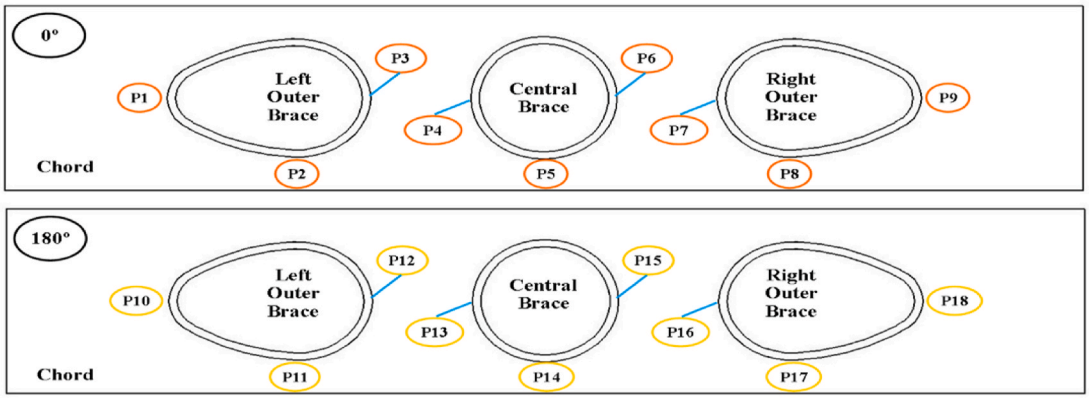

Fig. 5. The location of extraction SCF points in the uniplanar DKT-joints.

$$L_w = \frac{t}{2}\left[\frac{135^\circ - \psi\ (\text{deg.})}{45^\circ}\right] \tag{3}$$

The definition of H_w and L_w is represented in Fig. 7. In the study, the weld profile is modelled according to AWS [49] recommendations. It is a manifest fact that the modelled weld profile is usually different from the actual weld profile. Thus, for the amendment of SCFs to consider the actual weld toe position, the reader is referred to API RP2A section C 5.3.2 [45].

To model the weld profile, brace, chord, and FRP element type, solid 186 and SHELL 281 are utilized. The solid 186 element consists of 20 nodes with three degrees of freedom per node, which have compatible displacements and are well-suited to curved model boundaries. The SHELL 281 element has eight nodes with six degrees of freedom per node which has deformation and rotation in each node. To guarantee the quality of the mesh, the sub-zone technique is used. In this approach, each FE model is divided into different parts, which helps to improve the mesh quality in essential parts, such as the hot-spot region and the weld profile (Fig. 8).

Before conducting the parameter study, a convergence investigation is performed on the mesh topology to select the optimal number of elements through the chord thickness. Results of the convergence investigation are presented in Table 3. For the sake of brevity, the results of four FE models are presented, which indicates that the maximum change is about 4.3%; hence, two elements are selected (Fig. 8).

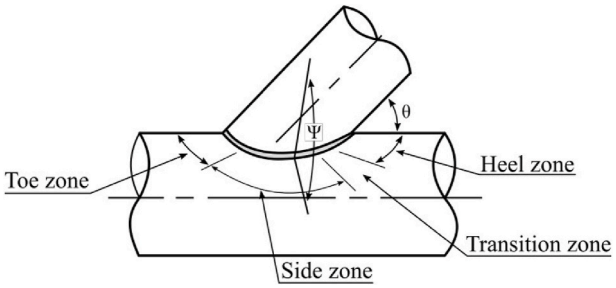

Fig. 6. Definition of dihedral angle Ψ based on AWS (2002).

2.3. FRP and uniplanar DKT-joints modelling consideration

To model the interaction between FRP and the chord, as well as FRP and the braces, the accurate way is to use the ANSYS contact capability. Thus, the chord, the braces, the weld profile, and the FRP are meshed separately. The chord and braces' outer surfaces were defined as the contact (contact 174) surface and the FRP was introduced as the target (target 170) surface. To transfer loading and deformation among FRP, chord, and braces, flexible-to-flexible surface-to-surface contact elements were applied to model the interaction. Since SCFs are calculated from stresses in the hot spot area, an increase in FRP length has no effect on the hot spot stress [50]. The length of the strengthened region of the chord and braces is shown in Fig. 9.

The used FRP properties are presented in Table A-3 in the appendix. According to previous research [31], a fibre orientation of 90° and 0° on the chord have more significant effects on axial loading compared to other angles. Hence, a combination of these values has been considered. FRP orientations are presented in Table 4.

2.4. SCF calculation methodology

To calculate the joint's SCF, a static analysis is appropriate [51]. An SCF is defined as according to Refs. [3,52] as follows:

$$SCF = \frac{HSS}{\sigma_n} \tag{4}$$

$$\sigma_n = \frac{F}{\mathrm{A}} \tag{5}$$

where σ_n and HSS are the nominal stress and hot spot stress, and F is the axial force, and A represents the cross-section of the loaded brace, respectively. The hot spot stress (HSS) at the weld toe is calculated by the extrapolation method recommended by IIW [53]. Thus, HSS is predicted from 0.4 T to 1.4 T from the weld toe (Fig. 10). The stress at the weld (σ) is calculated as:

$$\sigma = 1.4\sigma_1 - 0.4\sigma_2 \tag{6}$$

where σ_1 and σ_2 represents the first and second extrapolation points, respectively.

3. Validation process

To check the accuracy of the analysis method, the weld size, the meshing approach, and mesh size, the FE models must be verified

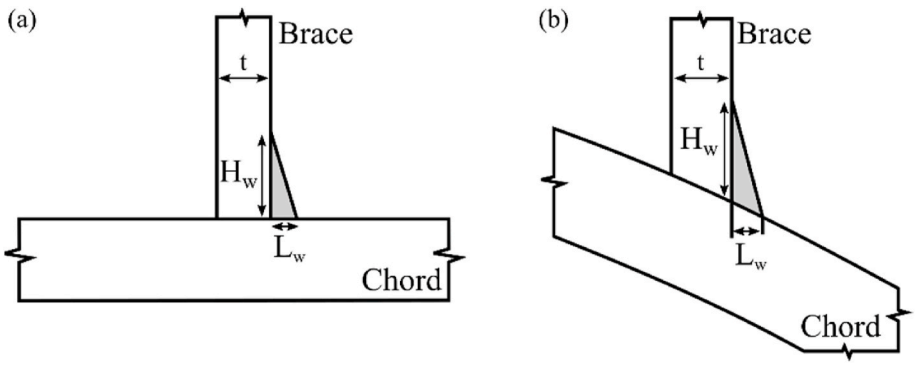

Fig. 7. Weld dimensions at (a) crown and (b) saddle locations [12].

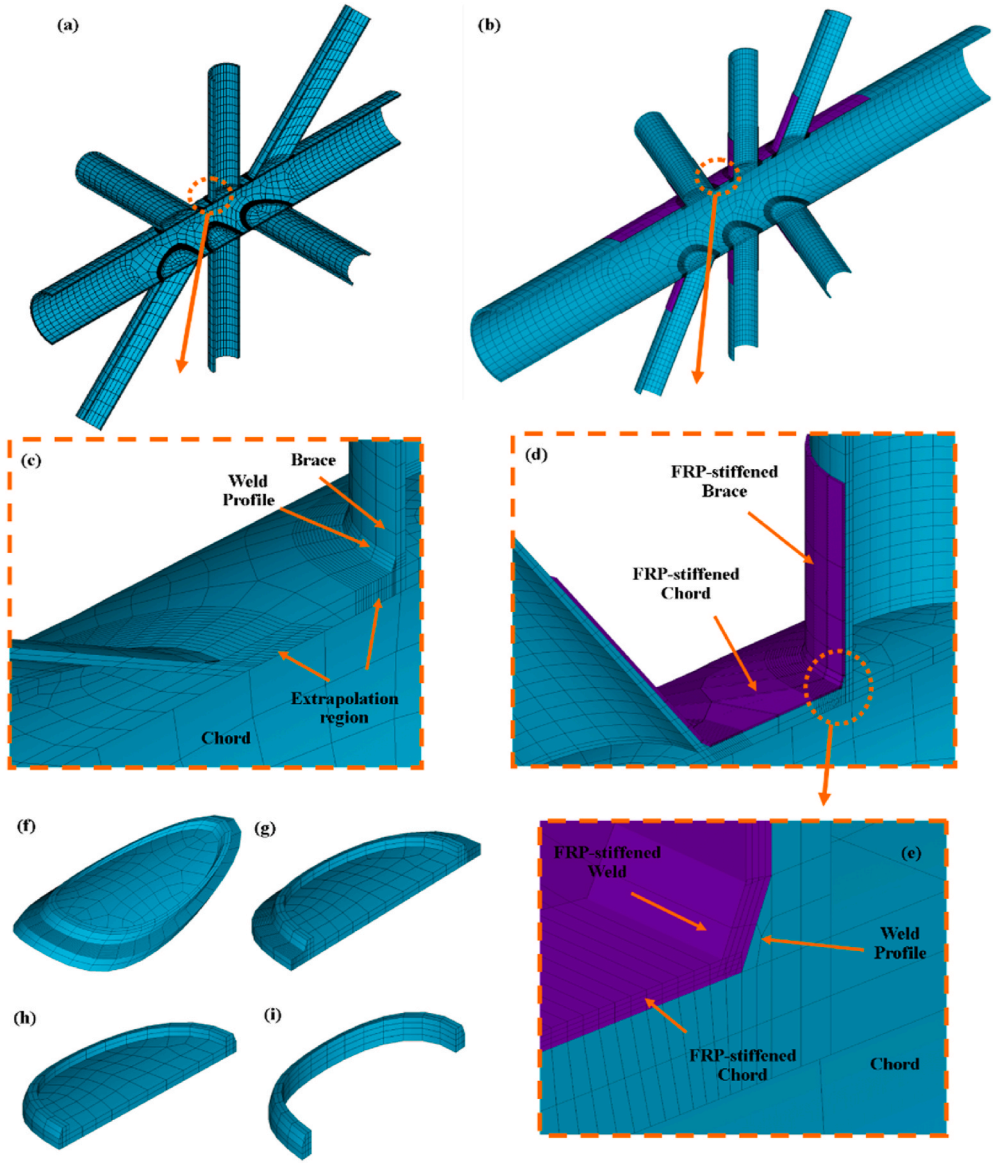

Fig. 8. The mesh generated by the sub-zone method: a) A view of the uniplanar DKT-joint; b) a view of the FRP-stiffened uniplanar DKT-joint; c) extrapolation region and weld profile; d) FRP-stiffened region; e) the FRP- stiffened weld profile; f) the outer brace extrapolation region; g) the central brace extrapolation region; h) plug area; i) a weld root.

by experimental data. To this end, experimental data, which are conducted by Lloyd's Register of Shipping OTH 354 [40], Chiew et al. [41], Lloyd's Register of Shipping OTH 353 [42], Hosseini et al. [43], Tong et al. [44] and formulas proposed by the LR equations [40], and API code [45] were utilized. The geometrical parameters of the validated joints and the belonging results are provided in Table 5, Table 6, and Table 7, respectively. The specimens from M1 to M16 were used to determine the SCFs in unreinforced tubular DKT-connections under axial loads which the maximum difference between the experimental and numerical results in 87% of models is about 14% in the saddle, crown heel, and crown toe positions. By closely looking at the results of these 16 models, it can be seen that the results of the SCFs in produced FE models and experimental models are close. The SCFs in reinforced tubular DKT connections under axial loads were predicted with the specimens from M17 to M24. The results of 8 reinforced models show that the maximum difference between the experimental and numerical results in 80% of models is less than 15%. Based on the validation of the models and Tables 6 and 7, there is a logical consensus between experimental and FE results. Accordingly, produced FE models are accurate enough to provide acceptable results in unreinforced and reinforced tubular DKT connections under axial loads.

Table 3
Comparison of the result of SCFs with a different number of elements through the chord thickness in the FE models subjected to the 1st, 3rd, 15th, and 16th loading condition.

Geometrical parameters	Number of elements	SCF value					$(SCF_{n\ elements}/SCF_{3\ elements}) - 1.0$				
		Outer brace			Central brace		Outer brace			Central brace	
		C_H	S	C_T	C	S	C_H	S	C_T	C	S
$\beta = 0.4$,	2	1.55	10.05	5.25	4.45	20.56	0.00%	0.00%	0.00%	0.00%	0.00%
$\gamma = 12$,	3	1.58	10.37	5.27	4.49	21.12	2.03%	3.15%	0.45%	0.98%	2.74%
$\tau = 1.0$,	4	1.60	10.43	5.30	4.50	21.22	3.45%	3.75%	1.12%	1.05%	3.20%
$\theta = 30^\circ$	5	1.62	10.46	5.31	4.50	21.22	4.21%	4.10%	1.20%	1.14%	3.22%
$\beta = 0.5$,	2	5.00	2.22	7.15	0.73	13.84	0.00%	0.00%	0.00%	0.00%	0.00%
$\gamma = 18$,	3	5.06	2.24	7.19	0.73	13.89	2.20%	2.65%	1.44%	0.84%	1.24%
$\tau = 7.0$,	4	5.12	2.25	7.19	0.73	14.00	3.50%	3.02%	1.37%	1.02%	2.02%
$\theta = 45^\circ$	5	5.00	2.22	7.15	0.73	13.84	1.04%	2.02%	0.80%	0.70%	0.90%
$\beta = 0.6$,	2	1.76	4.19	4.05	4.15	10.45	0.00%	0.00%	0.00%	0.00%	0.00%
$\gamma = 24$,	3	1.79	4.27	4.09	4.19	10.56	1.45%	1.87%	0.98%	0.87%	1.02%
$\tau = 0.4$,	4	1.79	4.28	4.12	4.21	10.61	1.32%	2.03%	1.65%	1.24%	1.54%
$\theta = 45^\circ$	5	1.81	4.31	4.13	4.23	10.66	2.60%	2.87%	2.01%	1.74%	2.03%
$\beta = 0.7$,	2	9.43	4.78	14.65	16.04	1.54	0.00%	0.00%	0.00%	0.00%	0.00%
$\gamma = 24$,	3	9.52	4.87	14.89	16.43	1.56	1.05%	1.87%	1.65%	2.45%	1.23%
$\tau = 1.0$,	4	9.54	4.91	15.00	16.53	1.58	1.22%	2.68%	2.41%	3.06%	2.74%
$\theta = 60^\circ$	5	9.67	4.97	15.15	16.71	1.59	2.54%	3.98%	3.45%	4.21%	3.08%

C: Crown, C_H: Crown Heel, C_T: Crown Toe, S: Saddle.

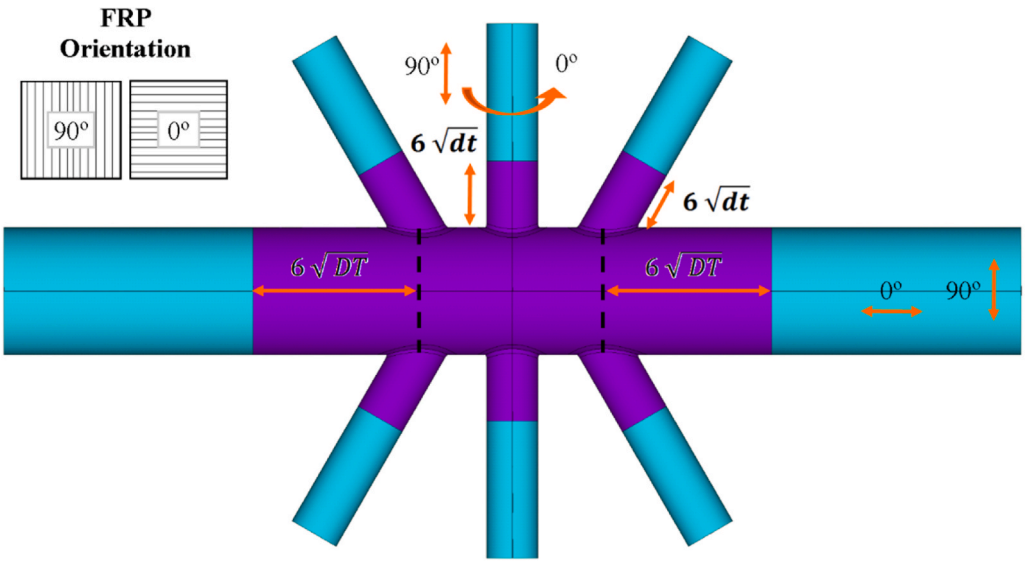

Fig. 9. The length of the strengthened region by FRP wrapping.

Table 4
FRP orientation schemes.

Pattern	4 layers	8 layers	12 layers	16 layers
1	[0°/0°/0°/0°]	2x[0°/0°/0°/0°]	3x[0°/0°/0°/0°]	4x[0°/0°/0°/0°]
2	[90°/90°/90°/90°]	2x[90°/90°/90°/90°]	3x[90°/90°/90°/90°]	4x[90°/90°/90°/90°]
3	[0°/90°/0°/90°]	2x[0°/90°/0°/90°]	3x[0°/90°/0°/90°]	4x[0°/90°/0°/90°]
4	[90°/0°/90°/0°]	2x[90°/0°/90°/90°]	3x[90°/0°/90°/90°]	4x[90°/0°/90°/90°]

4. SCF affecting parameters

4.1. Effects of FRP orientation on SCFs

Four FRP orientation patterns (Table 4) are investigated, and for the sake of brevity, only results of Carbon/epoxy (T300/5208) under 1st and 4th loading conditions are presented in Fig. 11, as the 2nd and 3rd loading conditions lead to equivalent conclusions. The

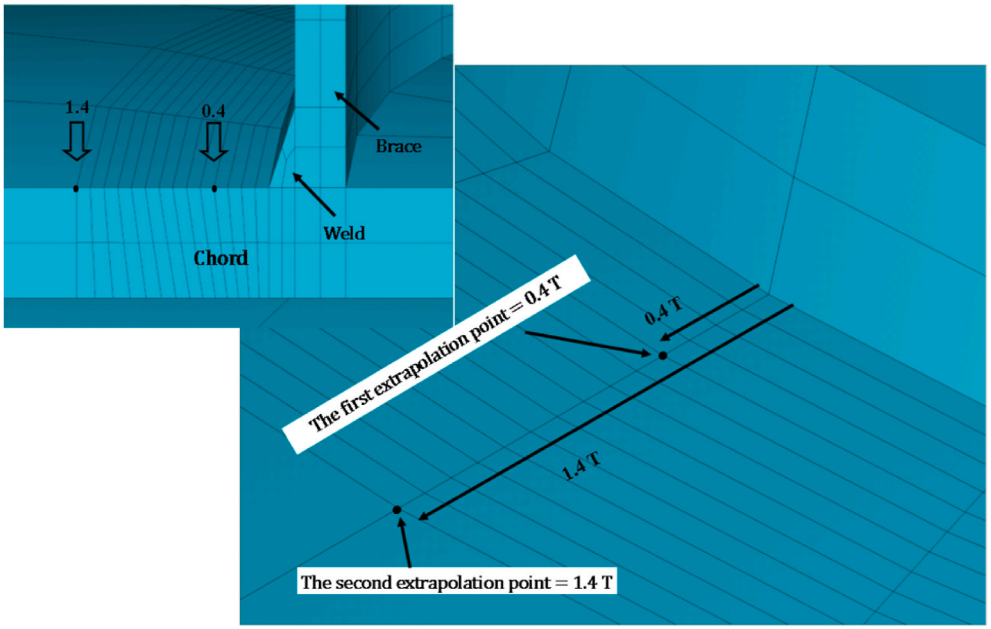

Fig. 10. The extrapolation points according to the IIW [53].

Table 5
Geometrical parameters of validation tests.

Number	Joint type	Type	Ref.	D (mm)	τ	β	γ	α	θ	ξ
M1	E30	X Un-reinforced	OTH 354 [40]	508	0.79	0.38	20.7	9.8	90	–
M2	B	X Un-reinforced	OTH 354 [40]	583	0.56	0.5	8.6	5.8	90	–
M3	X6	X Un-reinforced	OTH 354 [40]	407	0.81	0.35	25	17.5	90	–
M4	T204C	T Un-reinforced	OTH 354 [40]	914	0.5	0.5	14.3	5	90	–
M5	WE-Com	Multi-T Un-reinforced	Chiew et al. [41]	457	1.0	0.6	18.81	20.5	90	–
M6	7.A	K Un-reinforced	OTH 353 [42]	150	0.6	0.5	24	–	45	0.07
M7	6.B3	KT Un-reinforced	OTH 353 [42]	150	0.6	0.5	24	–	45	0.07
M8	6.A3	KT Un-reinforced	OTH 353 [42]	150	0.6	0.5	12	–	45	0.07
M9	T	T Un- and reinforced	Hosseini et al. [43]	328.3	1.00	0.67	25.90	12	90	–
M10	K1-13	K Un-reinforced	Tong et al. [44]	219	16.27	0.58	13.7	0.75	45	219
M11	K1-43	K Un-reinforced	Tong et al. [44]	219	16.27	0.58	13.7	0.75	45	219
M12	K1-23	K Un-reinforced	Tong et al. [44]	219	16.27	0.58	13.7	0.75	45	219
M13	K1-21	K Un-reinforced	Tong et al. [44]	219	16.27	0.58	13.7	0.75	45	219
M14	K1-25	K Un-reinforced	Tong et al. [44]	219	16.27	0.58	13.7	0.75	45	219
M15	K2-23	K Un-reinforced	Tong et al. [44]	219	16.27	0.58	18.25	0.7	45	219
M16	K3-23	K Un-reinforced	Tong et al. [44]	219	16.27	0.58	13.7	1	45	219
M17	CK1-13	K Reinforced	Tong et al. [44]	219	16.27	0.58	13.7	0.75	45	219
M18	CK1-43	K Reinforced	Tong et al. [44]	219	16.27	0.58	13.7	0.75	45	219
M19	CK1-23	K Reinforced	Tong et al. [44]	219	16.27	0.58	13.7	0.75	45	219
M20	CK1-21	K Reinforced	Tong et al. [44]	219	16.27	0.58	13.7	0.75	45	219
M21	CK1-25	K Reinforced	Tong et al. [44]	219	16.27	0.58	13.7	0.75	45	219
M22	CK2-23	K Reinforced	Tong et al. [44]	219	16.27	0.58	18.25	0.75	45	219
M23	CK3-23	K Reinforced	Tong et al. [44]	219	16.27	0.58	13.7	1	45	219
M24	CK4-23	K Reinforced	Tong et al. [44]	219	16.27	0.41	18.25	0.75	45	219

results indicate that at the crown heel position (P_1), the effects of all patterns are approximately similar, but at the crown toe (P_3) the third pattern leads to a more pronounced SCF reduction. At the saddle positions (P_2 and P_5), with 4 and 16 FRP layers, the third pattern leads to a higher reduction of the SCFs. However, with 8 and 12 FRP layers, the first and the third pattern have similar effects on the reduction of the SCFs. Hence, among the 4 ordination patterns, the third pattern is the most effective one. Therefore, the third pattern will be used for other parts of the presented research.

4.2. Effects of FRP materials on SCFs

The FRP materials that are used in the study, are shown in Table A-3 in the appendix. The reduction of the SCFs according to the use of different FRP materials is presented in Fig. 12. The horizontal axis indicates the investigated FRP materials, and the vertical axis

Table 6
Results of numerical and experimental tests in un-reinforced models.

Number	Position	Experimental	FE	API [45]	LR [40]	e1	e2	e3
M1	Saddle	21.80	20.00	15.68	14.47	9%	28%	38%
	Crown	3.30	3.65	4.20	4.56	−10%	−13%	−20%
M2	Saddle	4.80	4.77	4.52	3.72	1%	−5%	−22%
	Crown	–	2.24	1.94	2.44	–	−13%	9%
M3	Saddle	24	25.53	26.03	23.99	−6%	2%	−6%
	Crown	–	2.80	3.93	3.09	–	29%	10%
M4	Saddle	5.70	4.92	5.36	4.94	16%	9%	0%
	Crown	2.80	2.50	1.91	2.26	12%	−23%	−9%
M5	ws1ch	28.23	31.61	–	–	−11%	–	–
	ws2ch	20.04	21.30	–	–	−6%	–	–
M6	76	15.94	18.18	–	–	−12%	–	–
M7	4	14.78	17.01	–	–	−13%	–	–
	71	19.12	20.75	–	–	−8%	–	–
	94	21.97	22.94	–	–	−4%	–	–
	34	19.16	20.74	–	–	−8%	–	–
	82	19.37	22.62	–	–	−14%	–	–
M8	71	19.12	20.75	–	–	−8%	–	–
	94	21.97	22.94	–	–	−4%	–	–
	34	19.16	20.74	–	–	−8%	–	–
	82	19.37	22.62	–	–	−14%	–	–
M9	Crown	26.15	25.86	27.00	–	1%	4%	0%
	Saddle	4.97	5.32	5.08	5.73	−7%	−4%	8%
M10	COT	0.52	0.53	–	–	−1%	–	–
	C90T	3.25	3.17	–	–	3%	–	–
	C180T	3.72	3.26	–	–	12%	–	–
	COC	1.58	1.78	–	–	−13%	–	–
	C90C	2.94	3.08	–	–	−5%	–	–
	C180C	4.96	4.27	–	–	14%	–	–
M11	COT	0.45	0.47	–	–	−5%	–	–
	C90T	3.03	2.89	–	–	4%	–	–
	C180T	3.83	3.07	–	–	20%	–	–
	COC	1.77	1.83	–	–	−3%	–	–
	C90C	2.64	2.92	–	–	−11%	–	–
	C180C	4.21	4.09	–	–	3%	–	–
M12	COT	0.68	0.51	–	–	25%	–	–
	C90T	2.73	3.02	–	–	−11%	–	–
	C180T	3.37	3.24	–	–	4%	–	–
	COC	1.79	2.18	–	–	−22%	–	–
	C90C	3.12	3.04	–	–	3%	–	–
	C180C	3.2	3.85	–	–	−20%	–	–
M13	COT	0.62	0.59	–	–	5%	–	–
	C90T	2.81	3.05	–	–	−9%	–	–
	C180T	3.08	3.34	–	–	−9%	–	–
	COC	1.31	1.57	–	–	−20%	–	–
	C90C	2.62	3.18	–	–	−21%	–	–
	C180C	3.34	3.96	–	–	−19%	–	–
M14	COT	0.83	0.75	–	–	10%	–	–
	C90T	3.16	3.41	–	–	−8%	–	–
	C180T	2.94	2.87	–	–	2%	–	–
	COC	1.65	1.44	–	–	13%	–	–
	C90C	2.62	2.12	–	–	19%	–	–
	C180C	3	3.54	–	–	−18%	–	–
M15	COT	1.12	0.96	–	–	15%	–	–
	C90T	4.09	4.75	–	–	−16%	–	–
	C180T	3.59	3.41	–	–	5%	–	–
	COC	2.6	2.01	–	–	23%	–	–
	C90C	4.14	4.61	–	–	−11%	–	–
	C180C	3.42	3.07	–	–	10%	–	–
M16	COT	1.28	1.11	–	–	13%	–	–
	C90T	4.41	3.87	–	–	12%	–	–
	C180T	4.01	3.95	–	–	1%	–	–
	COC	2.46	2.10	–	–	15%	–	–
	C90C	4.81	4.71	–	–	2%	–	–
	C180C	5.83	5.14	–	–	12%	–	–

SCF_S = SCF in the saddle position; SCF_c = SCF in the crown position; S = saddle; C = Crown; e1 = ($SCF_{Experimental}$ -SCF_{FE}) - 1.0; (SCF_{API}/SCF_{FE}) - 1.0; (SCF_{LR}/SCF_{FE}) - 1.0.

Table 7
Results of numerical and experimental tests in reinforced models.

Number	Position	SCF		e1
		Experimental	FE	
M9	Phase 1 Saddle	25.23	24.63	2.44%
	Phase 2 Saddle	25.21	24.64	2.31%
	Phase 3 Saddle	18.27	17.61	3.75%
	Phase 1 Crown	4.86	5.10	−4.71%
	Phase 2 Crown	5.25	5.11	2.74%
	Phase 3 Crown	4.33	4.26	1.64%
M17	COT	0.59	0.87	−32.18%
	C90T	2.78	2.89	−3.81%
	C180T	3.02	3.45	−12.46%
	COC	1.54	1.44	6.94%
	C90C	2.4	2.23	7.62%
	C180C	3.68	3.18	15.72%
M18	COT	0.11	0.18	−38.89%
	C90T	2.47	2.75	−10.18%
	C180T	3.11	3.22	−3.42%
	COC	1.25	1.37	−8.76%
	C90C	2.06	2.33	−11.59%
	C180C	3.62	3.31	9.70%
M19	COT	0.37	0.45	−17.78%
	C90T	2.27	2.45	−7.35%
	C180T	2.96	3.39	−12.68%
	COC	1.62	1.82	−10.99%
	C90C	2.36	2.45	−3.67%
	C180C	2.51	2.6	−3.46%
M20	COT	0.63	0.84	−25.00%
	C90T	2.52	2.81	−10.32%
	C180T	2.81	3.21	−12.46%
	COC	1.41	1.68	−16.07%
	C90C	2.37	2.62	−9.54%
	C180C	2.58	2.44	5.74%
M21	COT	0.61	0.87	−29.89%
	C90T	2.48	2.34	5.98%
	C180T	2.6	2.91	−10.65%
	COC	1.47	1.92	−22.63%
	C90C	1.88	2.21	−14.93%
	C180C	2.1	1.89	11.11%
M22	COT	0.45	0.74	−39.19%
	C90T	2.95	3.31	−10.88%
	C180T	2.78	3.04	−8.55%
	COC	1.6	1.85	−13.51%
	C90C	3.09	3.45	−10.43%
	C180C	3.14	2.83	10.95%
M23	COT	0.93	0.87	6.90%
	C90T	3.72	3.45	7.83%
	C180T	3.7	3.12	18.59%
	COC	2.37	2.65	−10.57%
	C90C	3.87	4.21	−8.08%
	C180C	4.35	4.93	−11.22%
M24	COT	0.95	1.42	−33.10%
	C90T	3.28	3.1	5.81%
	C180T	3.77	3.67	2.72%
	COC	1.84	1.97	−6.60%
	C90C	3.43	3.21	6.85%
	C180C	3.9	4.31	−9.51%

$e1 = (SCF_{Experimental}/SCF_{FE}) - 1.0$.

shows the reduction of $SCF_{Un\text{-}strengthened}$ to $SCF_{FRP\text{-}strengthened}$ (S_R) in per cent. Regardless of the fibre orientation, using FRPs with increased mechanical properties, the reduction due to FRP reinforcement increases. As can be seen, Glass/vinyl ester with lower mechanical properties leads to the lowest SCF reduction of about 4%, while Carbon/epoxy (T300/5208) with higher mechanical properties has a more pronounced effect of approximately 10.2–43% reduction. Hence, carbon-based materials (CFRP) are 3–3.5 times more effective in reducing SCFs compared to glass-based materials (GFRP) at critical positions (crown and saddle points). A stiffer FRP has a higher contribution to the overall stiffness of the joint. A linear or exponential correlation of the FRP stiffness can be drawn from the results.

According to the analysis and Fig. 12, there is no significant difference between the effects of studied glass-based and carbon-based FRP. Thus, among three glass-based FRP, just effects of Glass/vinyl ester, and among two carbon-based FRPs, just the effects of Carbon/

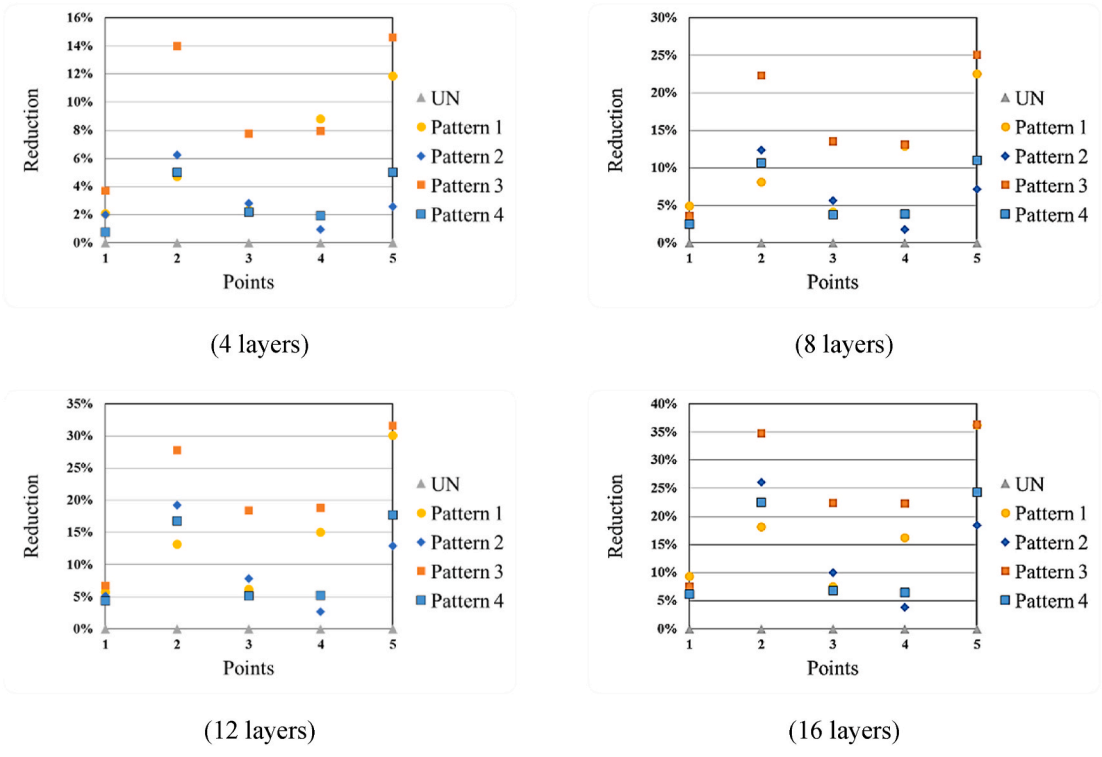

Fig. 11. Effects of different FRP orientation on SCFs in uniplanar DKT-joints at 1st and 4th loading condition, Carbon/epoxy (T300/5208), ($\tau = 0.7$, $\beta = 0.7$, $\theta = 45°$, $\gamma = 12$).

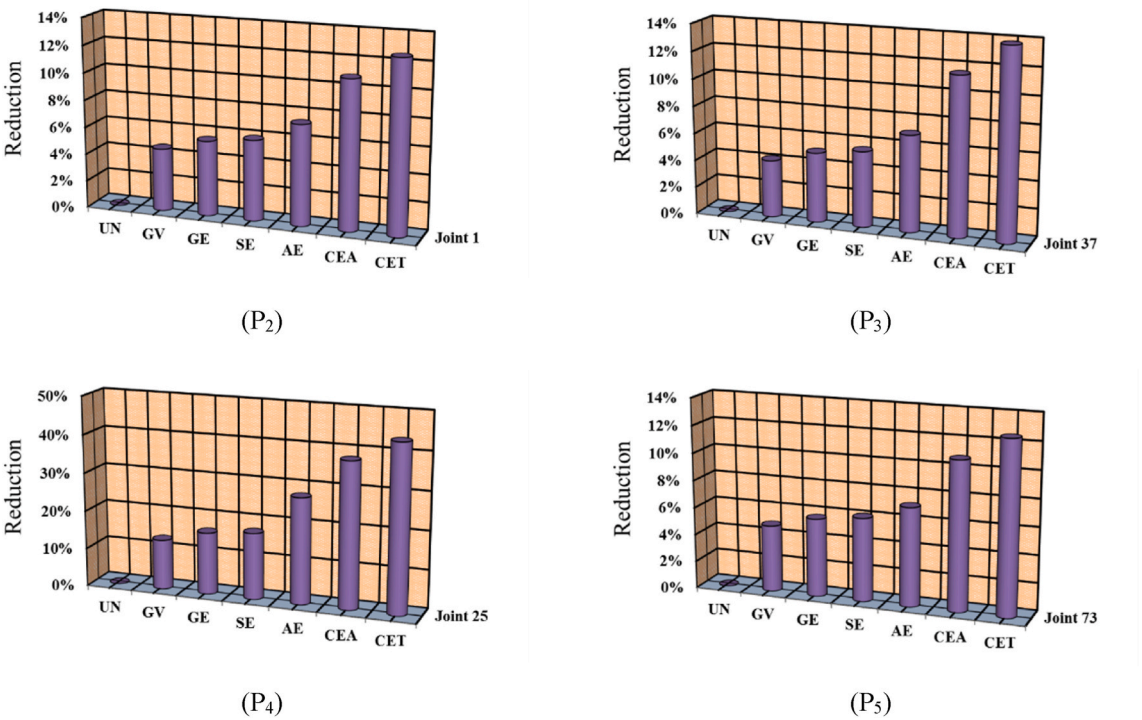

Fig. 12. Effects of different FRP materials on SCFs in uniplanar DKT-joints with 4 FRP layers; UN= Unstiffened joint; GV = Glass/vinyl ester; GE = Glass/epoxy (Scotchply 1002); SE= S-glass/epoxy; AE = Aramid/epoxy (Kevlar 9/Epoxy); CEA= Carbon/Epoxy (AS/3501); CET= Carbon/epoxy (T300/5208).

epoxy (T300/5208), will be investigated. Accordingly, three FRP materials, Glass/vinyl ester, Aramid/epoxy (Kevlar 9/Epoxy), and Carbon/epoxy (T300/5208) will be considered for other parts of the presented study.

4.3. Effects of β on SCFs in FRP-strengthened joints

The ratio of the brace diameter to the chord diameter is defined as β, *and* the influence on the SCFs of a DKT-joints is discussed in the following. When all braces are loaded by compression or all braces are loaded by tension, an increase of β leads to decreasing SCFs in all critical points. However, when some of the braces are loaded by compression and others are loaded by tension, an increase of β leads to decreasing SCFs at the saddle positions and increasing SCFs at the crown positions. Figs. 13 and 14 present the effects of β and the number of FRP layers on the SCFs. According to Fig. 13, an increasing β leads to decreasing SCFs in unstiffened joints and stiffened joints without considering the number of fibre layers at crown and saddle positions under the 1st loading condition. The decrease of SCFs at high values of β is more significant than at low values. According to Fig. 14, an increase of β leads to decreasing SCFs in unstiffened and stiffened joints without considering the number of layers at the saddle position and to an increasing SCF at the crown positions under the 4th loading pattern.

4.4. Effects of γ on SCFs in FRP-strengthened joints

The effects of the diameter-to-thickness ratio γ on the SCFs while additionally changing the number of layers are presented in Figs. 15 and 16. It can be seen that an increasing γ leads to increasing SCFs for the saddle position. Its reduction effect on the saddle position is significantly larger in higher values of γ with a small number of FRP layers. In contrast, an increasing γ leads to decreasing SCFs at the crown points. However, the effect of γ on the crown points is negligible, especially at lower values of γ with fewer FRP layers.

4.5. Effects of τ on SCFs in FRP-strengthened joints

The ratio of the thickness of the brace to the thickness of the chord is defined as τ ($\tau = t/T$). This section presents the effect of τ on the SCFs. This result is not dependent on the values of other geometrical parameters. Figs. 17 and 18 indicate that an increase of τ results in a rise in the SCFs in all loading conditions with different layers and different materials. It can be seen that a rise in the number of FRP layers leads to decreasing SCFs. This effect, caused by the FRP layers is significant in joints with higher τ. A total number of 16 layers is a suitable choice to decrease the SCFs of the DKT joint. Therefore, the utilization of FRP can improve the fatigue life of the structures.

4.6. Effects of θ on SCFs in FRP-strengthened joints

The effects of the inclination angle θ and the interaction of this parameter with the number of FRP layers on the SCFs are presented in Figs. 19 and 20. The results reveal that the increase of inclination angle leads to a decrease of SCFs values at the crown points and increasing SCF values at the saddle points in all loading conditions with different FRP materials and the number of layers. In addition, a rise in the number of FRP layers leads to decreasing SCFs. This result is not dependent on the values of other geometrical parameters.

5. Parametric equations

Parametric formulae are proposed to calculate the SCFs at crown and saddle positions of FRP-strengthened tubular DKT joints subjected to different axial loading conditions. The equations are obtained with multiple nonlinear regression analyses conducted by the statistical software package, SPSS. To this end, dimensionless parameters corresponding to the joint geometry (i.e., β, γ, τ, and θ) and FRP (η, ξ), and SCF are defined as the independent and dependent variables, respectively. A model of expression was built with dimensionless parameters and unknown coefficients. The parametric equations to predict the highest SCFs at crown and saddle positions are presented as follows, and to calculate SCFs in other locations, the related equations presented in the appendix:

- 1st loading condition

$$SCF_{1st-P2} = \left(0.344\tau^{1.115}\gamma^{0.1.242}\beta^{-0.446}\theta^{1.253}\xi^{-0.107}\eta^{-0.205}\right);\ R^2 = 0.968 \tag{7}$$

$$SCF_{1st-P5} = \left(0.477\tau^{1.013}\gamma^{1.278}\beta^{-0.225}\theta^{0.259}\xi^{-0.105}\eta^{-0.205}\right);\ R^2 = 0.961 \tag{8}$$

- 2nd loading condition

$$SCF_{2nd-P5} = \left(0.808\tau^{0.87}\gamma^{0.947}\beta^{0.131}\theta^{-0.182}\xi^{-0.104}\eta^{-0.128}\right);\ R^2 = 0.887 \tag{9}$$

$$SCF_{2nd-P12} = \left(10.189\tau^{1.135}\gamma^{-0.032}\beta^{0.145}\theta^{0.093}\xi^{-0.071}\eta^{-0.044}\right);\ R^2 = 0.941 \tag{10}$$

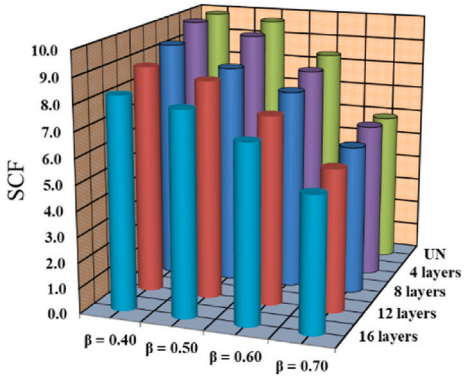

Fig. 13. Effects of β on SCFs in uniplanar DKT-joints at P_2 under the 1st loading condition ($\tau = 0.7$, $\theta = 30$, $\gamma = 18$, Glass/vinyl ester, the third orientation pattern).

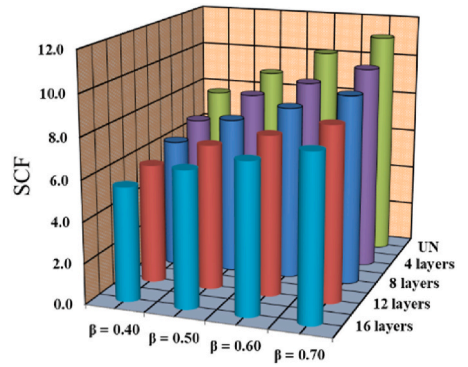

Fig. 14. Effects of β on SCFs in uniplanar DKT-joints at P_3 under the 4th loading condition ($\tau = 0.7$, $\theta = 60$, $\gamma = 24$, Carbon/epoxy (T300/5208), the third orientation pattern).

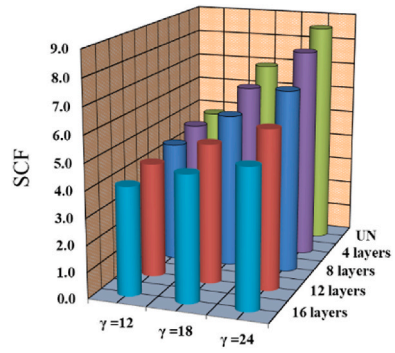

Fig. 15. Effects of γ on SCFs in uniplanar DKT-joints at P_5 under the 2nd loading condition ($\tau = 0.4$, $\theta = 45$, $\beta = 0.4$, Carbon/epoxy (T300/5208), the third orientation pattern).

$$SCF_{2nd-P13} = \left(16.852\tau^{1.119}\gamma^{-0.126}\beta^{0.356}\theta^{0.412}\xi^{-0.049}\eta^{-0.011}\right);\ R^2 = 0.943 \tag{11}$$

$$SCF_{2nd-P14} = \left(0.302\tau^{0.935}\gamma^{1.225}\beta^{-0.418}\theta^{0.048}\xi^{-0.119}\eta^{-0.155}\right);\ R^2 = 0.918 \tag{12}$$

- 3rd loading condition

$$SCF_{3rd-P4} = \left(16.091\tau^{1.096}\gamma^{-0.006}\beta^{0.547}\theta^{0.244}\xi^{-0.062}\eta^{-0.035}\right);\ R^2 = 0.951 \tag{13}$$

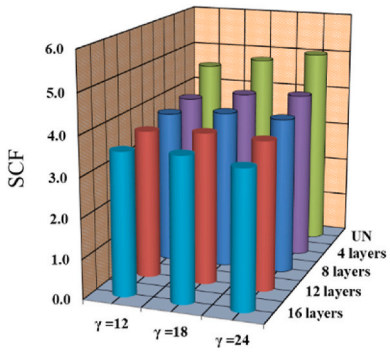

Fig. 16. Effects of γ on SCFs in uniplanar DKT-joints at P_{15} under the 3rd loading condition ($\tau = 0.4$, $\theta = 60$, $\beta = 0.6$, Carbon/epoxy (T300/5208), the third orientation pattern).

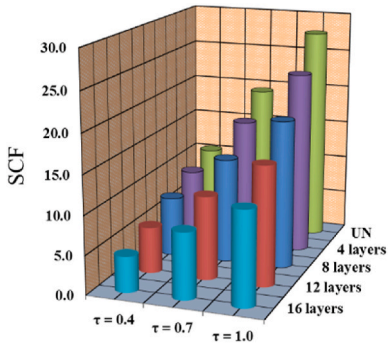

Fig. 17. Effects of τ on SCFs in uniplanar DKT-joints at P_{14} under the 2nd loading condition ($\gamma = 24$, $\theta = 60$, $\beta = 0.7$, Glass/vinyl ester, the third orientation pattern).

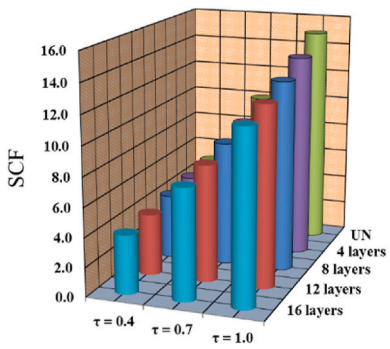

Fig. 18. Effects of τ on SCFs in uniplanar DKT-joints at P_3 under the 4th loading condition ($\gamma = 18$, $\theta = 30$, $\beta = 0.6$, Carbon/Epoxy (AS/3501), the third orientation pattern).

$$SCF_{3rd-P12} = \left(21.007\tau^{1.160}\gamma^{-0.164}\beta^{0.51}\theta^{-0.056}\xi^{-0.066}\eta^{-0.031}\right);\ R^2 = 0.938 \tag{14}$$

$$SCF_{3rd-P15} = \left(17.715\tau^{1.118}\gamma^{-0.123}\beta^{0.374}\theta^{0.162}\xi^{-0.049}\eta^{-0.019}\right);\ R^2 = 0.922 \tag{15}$$

$$SCF_{3rd-P16} = \left(13.370\tau^{1.164}\gamma^{-0.051}\beta^{0.344}\theta^{-0.102}\xi^{-0.077}\eta^{-0.05}\right);\ R^2 = 0.935 \tag{16}$$

- 4th loading condition

$$SCF_{4th-P3} = \left(20.051\tau^{1.165}\gamma^{-0.09}\beta^{0.521}\theta^{0.065}\xi^{-0.093}\eta^{-0.069}\right);\ R^2 = 0.949 \tag{17}$$

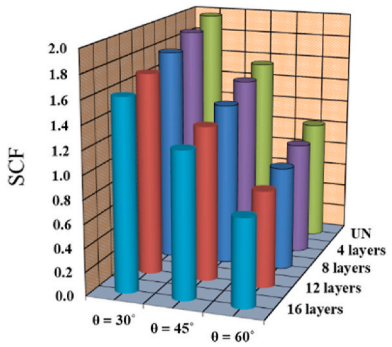

Fig. 19. Effects of θ on SCFs in uniplanar DKT-joints at P_3 under the 1st loading condition ($\gamma = 12$, $\tau = 0.4$, $\beta = 0.6$, Aramid/epoxy (Kevlar 9/Epoxy), the third orientation pattern).

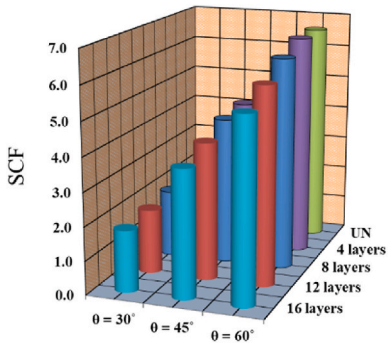

Fig. 20. Effects of θ on SCFs in uniplanar DKT-joints at P_8 under the 3rd loading condition ($\gamma = 24$, $\tau = 0.4$, $\beta = 0.4$, Aramid/epoxy (Kevlar 9/Epoxy), the third orientation pattern).

Table 8
Controlling the acceptance criteria of the Fatigue Guidance Review Panel [54], and the statistical indices for the SCF formulas.

Equation	Acceptance criteria [54]		Decision
	$\%P/R < 0.8$	$\%P/R > 1.5$	
(7)	$0\% \leq 5\%$	$1\% \leq 50\%$	Acceptable
(8)	$0\% \leq 5\%$	$0\% \leq 50\%$	Acceptable
(9)	$5\% \leq 5\%$	$1\% \leq 50\%$	Acceptable
(10)	$0\% \leq 5\%$	$1\% \leq 50\%$	Acceptable
(11)	$1\% \leq 5\%$	$2\% \leq 50\%$	Acceptable
(12)	$3\% \leq 5\%$	$0\% \leq 50\%$	Acceptable
(13)	$1\% \leq 5\%$	$2\% \leq 50\%$	Acceptable
(14)	$5\% \leq 5\%$	$1\% \leq 50\%$	Acceptable
(15)	$6\% \leq 5\%$	$3\% \leq 50\%$	Revise
(16)	$4\% \leq 5\%$	$2\% \leq 50\%$	Acceptable
(17)	$1\% \leq 5\%$	$2\% \leq 50\%$	Acceptable
(18)	$1\% \leq 5\%$	$2\% \leq 50\%$	Acceptable
(19)	$0\% \leq 5\%$	$0\% \leq 50\%$	Acceptable

$$SCF_{4th-P4} = \left(22.377\tau^{1.119}\gamma^{-0.102}\beta^{0.596}\theta^{0.244}\xi^{-0.084}\eta^{-0.054}\right);\ R^2 = 0.951 \tag{18}$$

The value of the maximum SCF in FRP-reinforced tubular DKT-joints under axial loads can be calculated as follows:

$$SCF_{max} = \left(0.499\tau^{1.013}\gamma^{1.266}\beta^{-0.218}\theta^{0.257}\xi^{-0.104}\eta^{-0.203}\right);\ R^2 = 0.961 \tag{19}$$

The range of validity of the SCF equations based on the numerical parametric studies is as Table 1.

6. Applicability control for the proposed formulae

The Fatigue Guidance Review Panel [54] criteria are used to check the reliability of the equations. Here P/R is the ratio of the

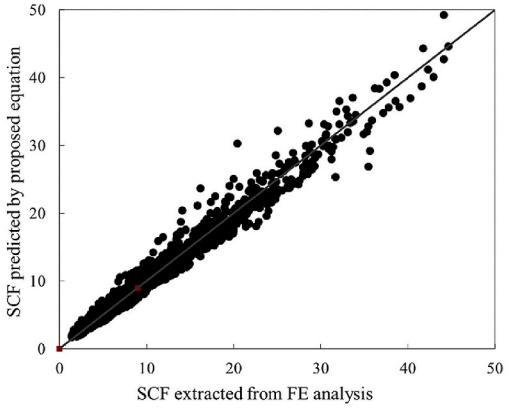

Eq. (7); 1st Ax loading condition

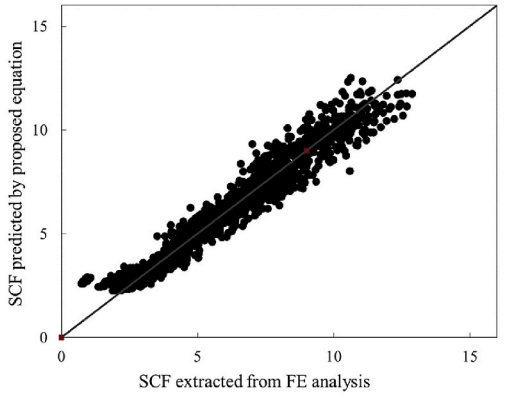

Eq. (16); 2nd Ax loading condition

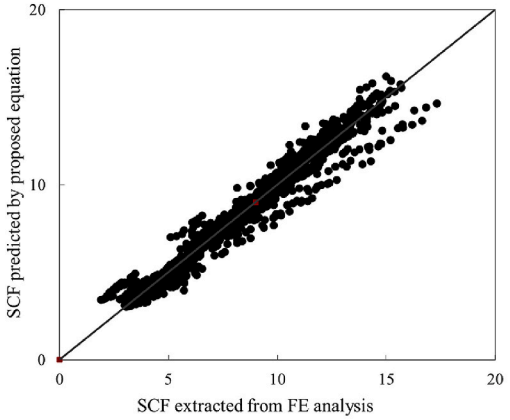

Eq. (13); 3rd Ax loading condition

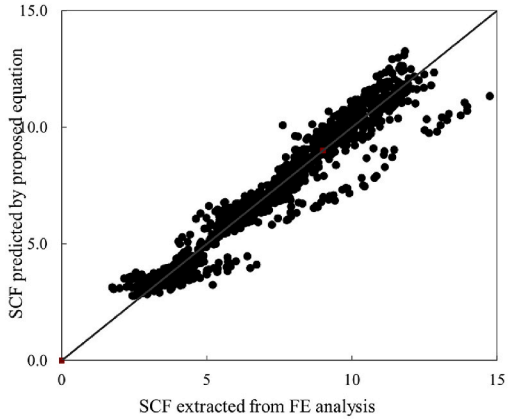

Eq. (15); 3rd Ax loading condition

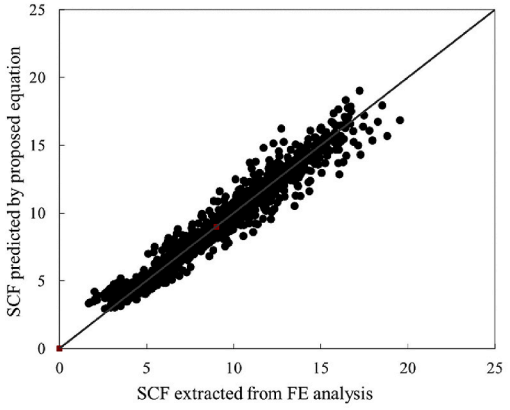

Eq. (18); 4th Ax loading condition

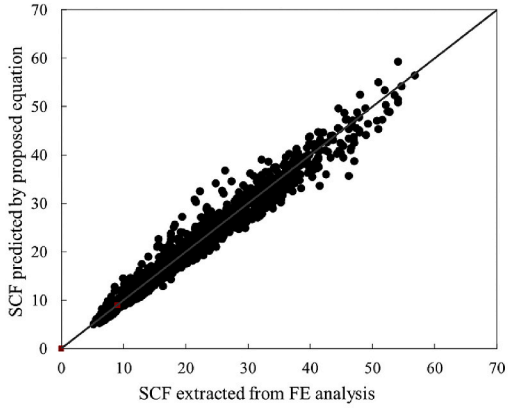

Eq. (19); Maximum SCF of FRP-reinforced tubular DKT-joints under axial loads

Fig. 21. The formulae predictions for the strengthened joints under axial loadings.

predicted SCF (P) from a given set of equations to the recorded SCF (R) from a test or analysis.

- The criteria for acceptable equations are $\%[P/R < 1.0] \leq 25\%$, and $\%[P/R < 0.8] \leq 5\%$.
- The criterion for conservative equations is $\%[P/R > 1.5] \geq 50\%$.
- The criteria for engineering judgment about equations are $25\% < \%[P/R < 1.0] \leq 30\%$, and/or $5\% < \%[P/R < 0.8] \leq 7.5\%$.
- Otherwise, equations are rejected.

Because for a mean fit equation, there is always a large percentage of under-prediction, the requirement for joint under-prediction, *i.e.* $P/R < 1.0$, can be removed entirely in the assessment of parametric equations. According to the Fatigue Guidance Review Panel [54], assessment results are presented in Table 8. As can be seen in this table, all of the proposed equations satisfy the criteria recommended by Fatigue Guidance Review Panel.

In Fig. 21, the SCF values predicted by the proposed equations are compared with the SCFs extracted from FE analyses. For the sake of brevity, only a few FE results are presented. It can be seen that there is a good agreement between the results of the proposed equations and numerically computed values.

As can be seen in Table 8, some equations satisfy the UK DoE criteria, but revision is required for equation (15). To revise equation (15), SCF values are multiplied by a coefficient in such a way that the obtained SCF set satisfies the UK DoE acceptance criteria. This idea can be expressed as follows [16]:

$$Design\ factor = \frac{SCF_{Design}}{SCF_{Eq}} \tag{20}$$

where values of SCF_{Eq} are calculated from the proposed equation, and the values of SCF_{Design} are expected to satisfy the UK DoE criteria. Multiple comparative analyses are carried out to determine the optimum values of the design factor. Hence, the following equations should be used for design purposes:

$$SCF_{Design} = 1.02 \times SCF_{3rd-P15} \tag{21}$$

It is worthy of mention that the obtained high coefficients of determination guarantee the accuracy of equations, and to augment the reliability of equations and to avoid any considerable under-prediction the design factor is presented.

7. Conclusions

The effects of FRP and dimensionless parameters on SCFs in FRP-stiffened DKT joints under axial loads are investigated. 108 FE models under 4 different axial loading conditions and strengthened by 6 different types of FRP materials are analysed in ANSYS. The main conclusions are summarized as follows:

- Among orientation patterns, the third pattern with zero and 90° of FRP orientation is the most effective one.
- Increasing the mechanical properties of FRP materials leads to an increasing influence of FRP. Hence, CFRPs with carbon-based materials are more effective and reduce SCFs about 3–3.5 times more than glass-based materials (GFRP).
- Increasing β leads to decreasing SCFs at the crown and saddle positions under the 1st loading condition. In addition, an increase of β leads to reducing SCFs at saddle positions and increasing SCFs at crown positions under the 4th loading condition.
- An increasing γ results in increasing SCFs at saddle positions and decreasing SCFs at crown points. The effects of γ on the crown points are negligible.
- An increase in τ results in increasing SCFs in all loading cases with different layers and materials.
- An increase in the inclination angle leads to decreasing SCFs at crown points and an increase at saddle points in all loading conditions.
- FRPs can decrease SCFs between 5 and 43%, which is a very large advantage for the fatigue life of tubular joints.
- Design formulae are proposed to calculate SCFs in FRP-reinforced tubular DKT joints under axial loads. Considering the relatively high values obtained for the coefficients of determination and the satisfaction of acceptance criteria recommended by the UK DoE, it can be concluded that the developed formulae can reliably be applied to predict the SCF in FRP-reinforced tubular DKT joints in engineering works.
- In this study, the effects of FRP and dimensionless parameters on SCFs in FRP-stiffened DKT joints under axial loads are investigated. However, the probability distribution can help to derive governing probability functions in the fatigue reliability analysis of tubular joints. Investigating the probability distribution of SCFs in FRP-stiffened DKT joints can be an important topic for future study

Declaration of competing interest

The authors declare that they have no known competing financial interests or personal relationships that could have appeared to influence the work reported in this paper.

Data availability

No data was used for the research described in the article.

Acknowledgements

This work contributes to the Strategic Research Plan of the Centre for Marine Technology and Ocean Engineering (CENTEC), which is financed by the Portuguese Foundation for Science and Technology (Fundação para a Ciência e Tecnologia - FCT) under contract UIDB/UIDP/00134/2020.

Appendix

Table A-1
Loading patterns

No Loading	Brace					
	A	B	C	D	E	F
1	1	1	1	1	1	1
2	−1	1	1	1	1	1
3	−1	1	−1	1	1	1
4	−1	1	1	1	−1	1
5	−1	1	−1	−1	1	1
6	1	−1	−1	−1	1	1
7	−1	1	−1	1	−1	1
8	−1	1	−1	−1	−1	1
9	−1	1	−1	−1	1	−1
10	−1	1	1	−1	1	1
11	−1	1	1	−1	−1	1
12	1	−1	1	1	1	1
13	1	−1	1	−1	−1	1
14	1	−1	−1	−1	−1	1
15	−1	−1	1	1	1	1
16	1	1	1	−1	−1	−1

1 = Compression, −1 = Tension.

Table A-2
SCF Extraction points in axially loaded uniplanar DKT-joints

Loading types	extraction points
1	P_1, P_2, P_3, P_4, P_5
2	P_1, P_2, P_3, P_4, P_5, P_{10}, P_{11}, P_{12}, P_{13}, P_{14}
3	All points
4	P_1, P_2, P_3, P_4, P_5

Table A-3
FRP materials specification used in the numerical parametric study [55,56].

Name	E_1 (MPa)	E_2 (MPa)	ν_{12}	ν_{32}	G_{12} (MPa)	G_{23} (MPa)
Glass/vinyl ester	28,000	7000	0.29	0.38	4500	2540
Glass/epoxy (Scotchply 1002)	38,600	8270	0.26	0.33	4140	3100
S-glass/epoxy	43,000	8900	0.27	0.4	4500	3180
Aramid/epoxy (Kevlar 9/Epoxy)	76,000	5500	0.34	0.37	2300	2010
Carbon/Epoxy (AS/3501)	138,000	8960	0.3	0.59	7100	2820
Carbon/epoxy (T300/5208)	181,000	10,300	0.28	0.59	7170	3240

Parametric formulae to calculate other points in uniplanar DKT-joints under axial loadings are presented in here:

- 1st loading condition

$$SCF_{1st-P1} = \left(0.598\tau^{0.940}\gamma^{0.160}\beta^{-1.7}\theta^{-0.994}\xi^{-1.128}\eta^{-0.176}\right)(0.092\xi\beta)(\eta+\eta)^{.085}1.889(\beta\gamma\theta)^{0.499}; R^2 = 0.606 \quad \text{(A-1)}$$

$$SCF_{1st-P3} = \left(0.316\tau^{1.010}\gamma^{0.489}\beta^{-0.712}\theta^{-0.748}\xi^{-0.148}\eta^{-0.233}\right) + (-0.272\xi\beta)(\eta+\eta)^{-3.361}2.934(\beta\gamma\theta)^{-1.491}; R^2 = 0.883 \quad \text{(A-2)}$$

$$SCF_{1st-P4} = \left(0.835\tau^{1.139}\gamma^{0.071}\beta^{-1.155}\theta^{-0.069}\xi^{-0.084}\eta^{-0.118}\right) + (0.004\xi\beta)(\eta+\eta)^{-1.887}0.004(\beta\gamma\theta)^{4.035}; R^2 = 0.843 \quad \text{(A-3)}$$

- 2nd loading condition

$$SCF_{2nd-P1} = \left(3.212\tau^{1.311}\gamma^{0.314}\beta^{-0.097}\theta^{0.884}\xi^{-0.044}\eta^{-0.023}\right);\ R^2 = 0.918 \tag{A-4}$$

$$SCF_{2nd-P2} = \left(0.089\tau^{3.297}\gamma^{-8.065}\beta^{-1.340}\theta^{7.850}\right)*(-0.073\xi\eta - 0.032\theta\xi + 0.065\tau + 0.233\theta - 0.182\tau\theta)(\gamma+\theta)^{9.689}(\tau+\beta)^{13.650}(\theta+\tau)^{-8.890}\left(\beta^{4.632}+\tau\theta\right)^{-5.945}; R^2 = 0.832 \tag{A-5}$$

$$SCF_{2nd-P3} = \left(18.48\tau^{1.059}\gamma^{-0.091}\beta^{0.427}\theta^{0.575}\xi^{-0.031}\eta^{0.013}\right);\ R^2 = 0.957 \tag{A-6}$$

$$SCF_{2nd-P4} = \left(0.003\tau^{1.388}\gamma^{2.003}\beta^{-1.018}\theta^{-0.516}\right) + (-0.106\gamma + 2.691\beta\tau - 0.465\tau + 2.706\theta - 1.816\tau\theta)(\gamma+\theta)^{-0.29}(\tau+\beta)^{3.703}(\theta+\tau)^{-0.286}\left(\eta^{-0.083}+\xi\eta\right)^{1.260}; R^2 = 0.787 \tag{A-7}$$

$$SCF_{2nd-P10} = \left(2.636\tau^{1.087}\gamma^{-0.182}\beta^{0.582}\theta^{-0.486}\right)(0.063\beta\theta - 5.855\beta - 1.088\tau\theta + 8.432\theta + 0.363\tau); R^2 = 0.954 \tag{A-8}$$

$$SCF_{2nd-P11} = \left(0.128\tau^{1.042}\gamma^{1.281}\beta^{-0.882}\theta^{1.09}\xi^{-0.127}\eta^{-0.171}\right);\ R^2 = 0.936 \tag{A-9}$$

- 3rd loading condition

$$SCF_{3rd-P1} = \left(4.344\tau^{1.235}\gamma^{0.167}\beta^{-0.201}\theta^{0.938}\xi^{-0.052}\eta^{-0.01}\right);\ R^2 = 0.907 \tag{A-10}$$

$$SCF_{3rd-P2} = \left(0.276\tau^{-2.569}\gamma^{-6.799}\beta^{-1.839}\theta^{3.083}\right)(0.001\eta + 0.117\beta\tau + 0.083\tau - 0.006\theta + 0.018\tau\theta)(\gamma+\theta)^{8.608}(\tau+\beta)^{7.455}(\theta+\tau)^{-5.072}\left(\eta^{-0.124}+\xi\eta\right)^{-1.151}; R^2 = 0.812 \tag{A-11}$$

$$SCF_{3rd-P3} = \left(16.594\tau^{1.121}\gamma^{-0.04}\beta^{0.504}\theta^{0.167}\xi^{-0.042}\eta^{-0.057}\right);\ R^2 = 0.931 \tag{A-12}$$

$$SCF_{3rd-P5} = \left(0.192\tau^{0.577}\gamma^{0.897}\beta^{-3.290}\theta^{-1.639}\xi^{-1.056}\eta^{-0.139}\right)(0.194\xi\beta)(\eta+\eta)^{-0.001}0.196(\beta\gamma\theta)^{0.719}; R^2 = 0.804 \tag{A-13}$$

$$SCF_{3rd-P6} = \left(15.735\tau^{1.081}\gamma^{-0.012}\beta^{0.493}\theta^{0.177}\xi^{-0.037}\eta^{-0.009}\right);\ R^2 = 0.950 \tag{A-14}$$

$$SCF_{3rd-P7} = \left(-6.162\tau^{0.946}\gamma^{0.516}\beta^{1.305}\theta^{0.214}\right) + (0.167\gamma + 38.721\beta\tau - 11.276\tau - 5.504\theta + 0.381\tau\theta) + (\gamma+\theta)^{0.505}(\tau+\beta)^{-0.384}(\theta+\tau)^{1.308}\left(\beta^{2.302}+\xi\eta\right)^{0.045}; R^2 = 0.934 \tag{A-15}$$

$$SCF_{3rd-P8} = \left(0.831\tau^{1.053}\gamma^{0.869}\beta^{0.161}\theta^{1.312}\xi^{-0.109}\eta^{-0.186}\right);\ R^2 = 0.961 \tag{A-16}$$

$$SCF_{3rd-P9} = \left(0.815\tau^{3.170}\gamma^{-1.191}\beta^{-4.520}\theta^{-0.277}\right) + (-0.033\gamma - 13.495\beta\tau - 8.160\tau - 0.126\theta\eta + 0.670\tau\theta)(\gamma+\theta)^{-1.207}(\tau+\beta)^{6.261}(\theta+\tau)^{-0.781}\left(\beta^{-4.287}+\xi\eta\right)^{1.306}; R^2 = 0.929 \tag{A-17}$$

$$SCF_{3rd-P10} = \left(16.137\tau^{1.218}\gamma^{-0.228}\beta^{0.257}\theta^{0.818}\xi^{-0.012}\eta^{0.039}\right);\ R^2 = 0.905 \tag{A-18}$$

$$SCF_{3rd-P11} = \left(-1.499\tau^{1.009}\gamma^{1.033}\beta^{2.891}\theta^{0.667}\right) + (0.009\eta + 0.057\beta\tau - 0.087\tau - 0.011\theta + 0.227\tau\theta)*(\gamma+\theta)^{1.434}(\tau+\beta)^{0.741}(\theta+\tau)^{-0.753}\left(\beta^{2.592}+\xi\eta\right)^{-0.309}; R^2 = 0.958 \tag{A-19}$$

$$SCF_{3rd-P13} = \left(21.349\tau^{1.123}\gamma^{-0.154}\beta^{0.536}\theta^{0.141}\xi^{-0.038}\eta^{-0.021}\right);\ R^2 = 0.918 \tag{A-20}$$

$$SCF_{3rd-P14} = \left(0.071\tau^{0.875}\gamma^{1.1.536}\beta^{-0.800}\theta^{0.191}\xi^{-0.139}\eta^{-0.235}\right);\ R^2 = 0.916 \tag{A-21}$$

$$SCF_{3rd-P17} = \left(0.125\tau^{1.037}\gamma^{1.321}\beta^{-0.612}\theta^{1.515}\xi^{-0.1337}\eta^{-0.240}\right);\ R^2 = 0.954 \tag{A-22}$$

$$SCF_{3rd-P18} = \left(24.383\tau^{1.034}\gamma^{-0.267}\beta^{0.381}\theta^{0.357}\right) + (0.117\eta - 17.202\beta\tau + 8.237\tau - 12.076\theta + 4.441\tau\theta)*(\gamma+\theta)^{-0.629}(\tau+\beta)^{4.048}(\theta+\tau)^{-2.108}\left(\beta^{-2.065}+\xi\eta\right)^{0.484}; R^2 = 0.958 \tag{A-23}$$

- 4th loading condition

$$SCF_{4th-P1} = \left(6.996\tau^{1.255}\gamma^{0.01}\beta^{-0.213}\theta^{0.802}\xi^{-0.057}\eta^{-0.004}\right);\ R^2 = 0.888 \tag{A-24}$$

$$SCF_{4th-P2} = \left(1.023\tau^{3.160}\gamma^{4.437}\theta^{6.835}\xi^{-1.485}\eta^{-0.577}\right)(1.026\xi\beta)(\xi+\eta)^{0.609}0.023(\beta\gamma\theta)^{-2.683}(\tau+\eta)^{0.578}(\theta+\tau)^{-2.683}\left(\eta^{4.691}+\tau\theta\right)^{-1.535};R^2=0.903 \tag{A-25}$$

$$SCF_{4th-P5} = \left(0.361\tau^{1.991}\gamma^{3.923}\theta^{3.019}\xi^{-1.544}\eta^{-15.065}\right)(0.362\xi\beta)(\xi+\eta)^{0.739}0.363(\beta\gamma\theta)^{-2.079}(\tau+\eta)^{-0.369}(\theta+\tau)^{-1.974}\left(\eta^{-4.753}+\tau\theta\right)^{-3.087};\ R^2 = 0.913 \tag{A-26}$$

The acceptance criteria of above equations presented in Table A-4.

Table A-4
Controlling the acceptance criteria of Fatigue Guidance Review Panel [54], and the statistical indices for the SCF formulas

Equation	Acceptance criteria [54]		Decision
	$\%P/R < 0.8$	$\%P/R > 1.5$	
(A-1)	21% ≤ 5%	16% ≤ 50%	Revision
(A-2)	7% ≤ 5%	6% ≤ 50%	Revision
(A-3)	8% ≤ 5%	4% ≤ 50%	Revision
(A-4)	4% ≤ 5%	12% ≤ 50%	Acceptable
(A-5)	17% ≤ 5%	17% ≤ 50%	Revision
(A-6)	0% ≤ 5%	1% ≤ 50%	Acceptable
(A-7)	14% ≤ 5%	14% ≤ 50%	Revision
(A-8)	8% ≤ 5%	5% ≤ 50%	Revision
(A-9)	5% ≤ 5%	3% ≤ 50%	Acceptable
(A-10)	5% ≤ 5%	12% ≤ 50%	Acceptable
(A-11)	10% ≤ 5%	21% ≤ 50%	Revision
(A-12)	3% ≤ 5%	2% ≤ 50%	Acceptable
(A-13)	11% ≤ 5%	21% ≤ 50%	Revision
(A-14)	2% ≤ 5%	2% ≤ 50%	Acceptable
(A-15)	12% ≤ 5%	8% ≤ 50%	Revision
(A-16)	4% ≤ 5%	1% ≤ 50%	Acceptable
(A-17)	14% ≤ 5%	9% ≤ 50%	Revision
(A-18)	6% ≤ 5%	7% ≤ 50%	Revise
(A-19)	7% ≤ 5%	6% ≤ 50%	Revise
(A-20)	6% > 5%	2% ≤ 50%	Revise
(A-21)	6% ≤ 5%	3% ≤ 50%	Revise
(A-22)	6% ≤ 5%	10% ≤ 50%	Revise
(A-23)	4% ≤ 5%	0% ≤ 50%	Acceptable
(A-24)	5% ≤ 5%	11% ≤ 50%	Acceptable
(A-25)	14% > 5%	22% ≤ 50%	Revise
(A-26)	14% > 5%	15% ≤ 50%	Revise

The design factors for revised formulae are as follows:

$$SCF_{Design} = 1.30 \times SCF_{1st-P1} \tag{A-27}$$

$$SCF_{Design} = 1.03 \times SCF_{1st-P3} \tag{A-28}$$

$$SCF_{Design} = 1.04 \times SCF_{1st-P4} \tag{A-29}$$

$$SCF_{Design} = 1.25 \times SCF_{2nd-P2} \tag{A-30}$$

$$SCF_{Design} = 1.10 \times SCF_{2nd-P4} \tag{A-31}$$

$$SCF_{Design} = 1.25 \times SCF_{2nd-P10} \tag{A-32}$$

$$SCF_{Design} = 1.13 \times SCF_{3rd-P2} \tag{A-33}$$

$$SCF_{Design} = 1.18 \times SCF_{3rd-P5} \tag{A-34}$$

$$SCF_{Design} = 1.18 \times SCF_{3rd-P7} \tag{A-35}$$

$$SCF_{Design} = 1.35 \times SCF_{3rd-P9} \tag{A-36}$$

$$SCF_{Design} = 1.03 \times SCF_{3rd-P10} \quad \text{(A-37)}$$

$$SCF_{Design} = 1.16 \times SCF_{3rd-P11} \quad \text{(A-38)}$$

$$SCF_{Design} = 1.02 \times SCF_{3rd-P13} \quad \text{(A-39)}$$

$$SCF_{Design} = 1.03 \times SCF_{3rd-P14} \quad \text{(A-40)}$$

$$SCF_{Design} = 1.02 \times SCF_{3rd-P17} \quad \text{(A-41)}$$

$$SCF_{Design} = 1.29 \times SCF_{4th-P2} \quad \text{(A-42)}$$

$$SCF_{Design} = 1.20 \times SCF_{4th-P5} \quad \text{(A-43)}$$

References

[1] Chang E, Dover WD. Prediction of stress distributions along the intersection of tubular Y and T-joints. Int J Fatig 1999;21(4):361–81. https://doi.org/10.1016/S0142-1123(98)00083-8.
[2] Fricke W. Fatigue analysis of welded joints: state of development. Mar Struct 2003;16(3):185–200. https://doi.org/10.1016/S0951-8339(02)00075-8.
[3] Zavvar E, Guedes Soares C. Effects of fibre reinforced polymer on stress concentration factors in uniplanar DKT-joints subjected to the compression loading. In: Soares Guedes, C Santos TA, editors. Trends in maritime Technology and engineering. London, UK: Taylor and Francis; 2022. p. 249–60.
[4] Gao F. Stress and strain concentrations of completely overlapped tubular joints under lap brace OPB load. Thin-Walled Struct 2006;44(8):861–71. https://doi.org/10.1016/j.tws.2006.08.017.
[5] Cheng B, Li C, Lou Y, Zhao X. Parametric FE modeling to predict hot spot stress concentrations of bird-beak SHS joints in offshore structures. Ocean Eng 2018;160:54–67. https://doi.org/10.1016/j.oceaneng.2018.04.077.
[6] Shao YB. Analysis of stress concentration factor of welded tubular K-joints subjected to axial loads. Chuan Bo Li Xue/Journal Sh Mech. 2010;14(4):399–408.
[7] Zhang J, Jiang J, Shen W, Luo Y. A novel framework for deriving the unified SCF in multi-planar overlapped tubular joints. Mar Struct 2018;60:72–86. https://doi.org/10.1016/j.marstruc.2018.03.008.
[8] Liu PH, Chen IY, Liu XQ, et al. Stress influence matrix on hot spot stress analysis for welded tubular joint in offshore jacket structure. Ocean Eng 2022;251:111103. https://doi.org/10.1016/j.oceaneng.2022.111103.
[9] Jiang Y, Yuan K, Cui H. Prediction of stress concentration factor distribution for multi-planar tubular DT-joints under axial loads. Mar Struct 2018;61:434–51. https://doi.org/10.1016/j.marstruc.2018.06.017.
[10] Lotfollahi-Yaghin MA, Ahmadi H. Geometric stress distribution along the weld toe of the outer brace in two-planar tubular DKT-joints: parametric study and deriving the SCF design equations. Mar Struct 2011;24(3):239–60. https://doi.org/10.1016/j.marstruc.2011.02.005.
[11] Ahmadi H, Zavvar E. The effect of multi-planarity on the SCFs in offshore tubular KT-joints subjected to in-plane and out-of-plane bending loads. Thin-Walled Struct 2016;106:148–65. https://doi.org/10.1016/j.tws.2016.04.020.
[12] Zavvar E, Hectors K, De Waele W. Stress concentration factors of multi-planar tubular KT-joints subjected to in-plane bending moments. Mar Struct 2021;78:103000. https://doi.org/10.1016/j.marstruc.2021.103000.
[13] Ahmadi H, Zavvar E. Degree of bending (DoB) in offshore tubular KT-joints under the axial, in-plane bending (IPB), and out-of-plane bending (OPB) loads. Appl Ocean Res 2020;95:102015. https://doi.org/10.1016/j.apor.2019.102015.
[14] Zavvar E, Ahmadi H. Degree of bending (Dob) induced by out-of-plane bending (OPB) loading in tubular KT-joints of jacket structures. 8th Int Offshore Ind Conf. Published online 2019.
[15] Ahmadi H, Yeganeh A, Mohammadi AH, Zavvar E. Probabilistic analysis of stress concentration factors in tubular KT-joints reinforced with internal ring stiffeners under in-plane bending loads. Thin-Walled Struct 2016;99:58–75. https://doi.org/10.1016/j.tws.2015.11.010.
[16] Ahmadi H, Zavvar E. Stress concentration factors induced by out-of-plane bending loads in ring-stiffened tubular KT-joints of jacket structures. Thin-Walled Struct 2015;91:82–95. https://doi.org/10.1016/j.tws.2015.02.011.
[17] Nassiraei H, Rezadoost P. SCFs in tubular X-joints retrofitted with FRP under out-of-plane bending moment. Mar Struct 2021;79:103010. https://doi.org/10.1016/j.marstruc.2021.103010.
[18] Soh AK, Soh CK. Stress analysis of axially loaded T tubular joints reinforced with doubler plates. Comput Struct 1995;55(1):141–9. https://doi.org/10.1016/0045-7949(94)00412-V.
[19] Nassiraei H, Lotfollahi-Yaghin MA, Neshaei SA, Zhu L. Structural behavior of tubular X-joints strengthened with collar plate under axially compressive load at elevated temperatures. Mar Struct 2018;61:46–61. https://doi.org/10.1016/j.marstruc.2018.03.012.
[20] Nassiraei H, Mojtahedi A, Lotfollahi-Yaghin MA. Static strength of X-joints reinforced with collar plates subjected to brace tensile loading. Ocean Eng 2018;161:227–41. https://doi.org/10.1016/j.oceaneng.2018.05.017.
[21] Cho KN, Ha WI, Jang CD, Kang SJ. Ultimate strength of specially reinforced tubular joint with brackets. Mar Struct 1991;4(1):57–79. https://doi.org/10.1016/0951-8339(91)90024-6.
[22] Qian X, Jitpairod K, Marshall P, et al. Fatigue and residual strength of concrete-filled tubular X-joints with full capacity welds. J Constr Steel Res 2014;100:21–35. https://doi.org/10.1016/j.jcsr.2014.04.021.
[23] Morahan DJ, van Foeken RJ, Lalani M, Wardenier J. New data on the fatigue and ultimate limit state of grouted tubular joints. In: Proceedings of the 1996 offshore Technology conference. Part 3 (of 4). vol. 2. Offshore Technol Conf; 1996. p. 467–71.
[24] Chen NZ, Guedes Soares C. Longitudinal strength analysis of ship hulls of composite materials under sagging moments. Compos Struct 2007;77(1):36–44. https://doi.org/10.1016/j.compstruct.2005.06.002.
[25] Weitzenböck JR, Hayman B, Hersvik G, et al. Application of composites in ships and offshore - a review and outlook. In: International conference on marine and offshore composites 2010; 2010. p. 1–39.
[26] Shi XH, Hu Z, Zhang J, Guedes Soares C. Ultimate strength of a cracked stiffened panel repaired by CFRP and stop holes. Ocean Eng 2021;226:108850. https://doi.org/10.1016/j.oceaneng.2021.108850.
[27] Zhao XL, Zhang L. State-of-the-art review on FRP strengthened steel structures. Eng Struct 2007;29(8):1808–23. https://doi.org/10.1016/j.engstruct.2006.10.006.
[28] T Y, Tj G, Wy L. Stress-Strain behavior of concrete in hybrid FRP-concrete-steel Double-skin tubular columns. J Struct Eng 2010;136(4):379–89. https://doi.org/10.1061/(ASCE)ST.1943-541X.0000121.

[29] Lin G, Zeng JJ, Teng JG, Li LJ. Behavior of large-scale FRP-confined rectangular RC columns under eccentric compression. Eng Struct 2020;216:110759. https://doi.org/10.1016/j.engstruct.2020.110759.
[30] Xu X, Shao Y, Gao X, Mohamed HS. Stress concentration factor (SCF) of CHS gap TT-joints reinforced with CFRP. Ocean Eng 2022;247:110722. https://doi.org/10.1016/j.oceaneng.2022.110722.
[31] Sadat Hosseini A, Zavvar E, Ahmadi H. Stress concentration factors in FRP-strengthened steel tubular KT-joints. Appl Ocean Res 2021;108(February):102525. https://doi.org/10.1016/j.apor.2021.102525.
[32] Nassiraei H, Rezadoost P. Stress concentration factors in tubular T/Y-joints strengthened with FRP subjected to compressive load in offshore structures. Int J Fatig 2020;140:105719. https://doi.org/10.1016/j.ijfatigue.2020.105719.
[33] Nassiraei H, Rezadoost P. Stress concentration factors in tubular T/Y-connections reinforced with FRP under in-plane bending load. Mar Struct 2021;76:102871. https://doi.org/10.1016/j.marstruc.2020.102871.
[34] Nassiraei H, Rezadoost P. Parametric study and formula for SCFs of FRP-strengthened CHS T/Y-joints under out-of-plane bending load. Ocean Eng 2021;221:108313. https://doi.org/10.1016/j.oceaneng.2020.108313.
[35] Zhao XL, Fernando D, Al-Mahaidi R. CFRP strengthened RHS subjected to transverse end bearing force. Eng Struct 2006;28(11):1555–65. https://doi.org/10.1016/j.engstruct.2006.02.008.
[36] Zavvar E, Sadat Hosseini A, Lotfollahi-Yaghin MA. Stress concentration factors in steel tubular KT-connections with FRP-Wrapping under bending moments. Structures 2021;33:4743–65. https://doi.org/10.1016/j.istruc.2021.06.100.
[37] Lesani M, Bahaari MR, Shokrieh MM. Numerical investigation of FRP-strengthened tubular T-joints under axial compressive loads. Compos Struct 2013;100:71–8. https://doi.org/10.1016/j.compstruct.2012.12.020.
[38] Nassiraei H, Rezadoost P. SCFs in tubular X-connections retrofitted with FRP under in-plane bending load. Compos Struct 2021;274:114314. https://doi.org/10.1016/j.compstruct.2021.114314.
[39] Nassiraei H, Rezadoost P. Stress concentration factors in tubular X-connections retrofitted with FRP under compressive load. Ocean Eng 2021;229:108562. https://doi.org/10.1016/j.oceaneng.2020.108562.
[40] Health and Safety Executive LR of S. Stress concentration factors for simple tubular joints – assessment of existing and development of new parametric formulae. 1997. OTH 354. Published online.
[41] Chiew SP, Soh CK, Wu NW. Experimental and numerical stress analyses of tubular XT-joint. J Struct Eng 1999;125(11):11. https://doi.org/10.1061/(ASCE)0733-9445(1999)125. 1239.
[42] Health and Safety Executive LR of S. Stress concentration factors for tubular complex joints. OTH 1992;91 353. Published online.
[43] Sadat Hosseini A, Bahaari MR, Lesani M. Experimental and parametric studies of SCFs in FRP strengthened tubular T-joints under axially loaded brace. Eng Struct 2020;213(October 2019):110548. https://doi.org/10.1016/j.engstruct.2020.110548.
[44] Tong L, Xu G, Zhao XL, Zhou H, Xu F. Experimental and theoretical studies on reducing hot spot stress on CHS gap K-joints with CFRP strengthening. Eng Struct 2019;201:109827. https://doi.org/10.1016/j.engstruct.2019.109827.
[45] American Petroleum Institute (API). Planning, designing, and constructing fixed offshore platforms—working stress design. 2020. Published online.
[46] Efthymiou M. Development of SCF formulae and generalised influence functions for use in fatigue analysis. Proc Conf Recent Dev Tubul Joints Technol 1988. Published online.
[47] Smedley P, Fisher P. Stress concentration factors for simple tubular joints. In: The first international offshore and polar engineering conference. International Society of Offshore and Polar Engineers; 1991.
[48] Zavvar E, Ahmadi H. Parametric study of degree of bending in tubular KT-joints under the IPB loading. Conf Int Conf Coasts, Ports Mar Struct (ICOPMAS 2018) Ports Marit Organ 2018. Published online.
[49] American Welding Society. Structural welding code. AWS. Published online. 2002.
[50] Sadat Hosseini A, Bahaari MR, Lesani M. Parametric study of FRP strengthening on stress concentration factors in an offshore tubular T-joint subjected to in-plane and out-of-plane bending moments. Int J Steel Struct 2019;19(6):1755–66. https://doi.org/10.1007/s13296-019-00244-0.
[51] N'Diaye A, Hariri S, Pluvinage G, Azari Z. Stress concentration factor analysis for welded, notched tubular T-joints under combined axial, bending and dynamic loading. Int J Fatig 2009;31(2):367–74. https://doi.org/10.1016/j.ijfatigue.2008.07.014.
[52] Zavvar E, Ahmadi H. Parametric study of stress concentration factors in three-planar tubular KT-joints subjected to out-of-plane bending loads. Conf Int Conf Coasts, Ports Mar Struct (ICOPMAS 2016) Ports Marit Organ 2016. Published online.
[53] IIW-XV-E. Recommended fatigue design procedure for welded hollow section joints. 1999. Published online.
[54] MaTSU. Fatigue background guidance document. HSE Books as a Offshore Technol Rep.; 1996. Published online.
[55] Kollar LP, Springer GS. Mechanics of composite structures. Cambridge university press; 2003.
[56] Bisby L, Kodur V, Green M. Performance of fire of FRP-confined reinforced concrete columns. 4th Int Conf Adv Compos Mater Bridg Struct. Published online 2004:1–8.